

Numerical Implementation of Anisotropic Damage Mechanics

John A. Nairn*, Chad C. Hammerquist, and Yamina E. Aimene

Wood Science and Engineering, Oregon State University, Corvallis, OR 97330, USA

SUMMARY

This paper describes implementation of anisotropic damage mechanics in the material point method (MPM). The approach was based on previously-proposed, fourth-rank anisotropic damage tensors. For implementation, it was convenient to recast the stress update using a new damage strain partitioning tensor. This new tensor simplifies numerical implementation (a detailed algorithm is provided) and clarifies the connection between cracking strain and an implied physical crack with crack opening displacements. By using two softening laws and three damage parameters corresponding to one normal and two shear cracking strains, damage evolution can be directly connected to mixed tensile and shear fracture mechanics. Several examples illustrate interesting properties of robust anisotropic damage mechanics such as modeling of necking, multiple cracking in coatings, and compression failure. Direct comparisons between explicit crack modeling and damage mechanics in the same MPM code show that damage mechanics can quantitatively reproduce many features of explicit crack modeling. A caveat is that strengths and energies assigned to damage mechanics materials must be changed from measured material properties to apparent properties before damage mechanics can agree with fracture mechanics.

Copyright © 0000 John Wiley & Sons, Ltd.

Received ...

KEY WORDS: Damage; Fracture; Particle methods; Constitutive equations; Stochastic problems

1. INTRODUCTION

Damage mechanics has a long history of modeling failure by augmenting material constitutive laws [1]. It has developed along two tracks. In one approach, damage is described as a second-rank tensor (like strain) and the constitutive law is modified to have stress related to both strain and damage requiring a new fourth-rank tensor for the damage term [2]. In an alternative track, stress (σ) is related to strain (ϵ) by

$$\sigma = (\mathbf{I} - \mathbf{D})\mathbf{C}_0(\epsilon - \alpha\Delta T) \quad (1)$$

where \mathbf{C}_0 is the undamaged material's fourth-rank stiffness tensor, \mathbf{D} is a fourth-rank damage tensor, and $\alpha\Delta T$ is residual thermal strain (or could be some other residual strain). The potential of this approach to model material failure rests in development of damage tensors \mathbf{D} that describe damage in real materials. In typical implementations, \mathbf{D} is reduced to one or more damage parameters. The models then propose criteria for initiation and evolution of those parameters. Most damage mechanics implementations use a single damage parameter, d_I , and

*Correspondence to: Wood Science and Engineering, Oregon State University, Corvallis, OR 97330, USA. Email: John.Nairn@oregonstate.edu

Contract/grant sponsor: National Institute of Food and Agriculture (NIFA) of the United States Department of Agriculture (USDA); contract/grant number: 2013-34638-21483

assume “isotropic” $\mathbf{D} = d_I \mathbf{I}$ [3, 4]. This “scalar damage” model scales all elements of \mathbf{C}_0 uniformly with evolution of d_I . Ju [5] argues that such scaling corresponds to a large representative volume element (RVE) with a random array of cracks. But, it is difficult to find any examples of materials that fail this way. Instead, initiation of damage usually results in coalescence of damage into dominate failure zones (e.g., cracks). Such zones cause any material to become anisotropic and therefore their modeling requires anisotropic methods.

Chaboche [6, 7, 8] proposed modeling damage-induced material anisotropy by using an anisotropic \mathbf{D} instead of the usual isotropic $d_I \mathbf{I}$. A material may start out as isotropic, but once damage initiates, an anisotropic \mathbf{D} converts it to an anisotropic material depending on damage orientation. Chaboche [6, 7, 8] proposed a specific form for \mathbf{D} that depends on three damage variables. Similarly, Ladèzeve and coworkers model anisotropic damage mechanics with two or more damage variables for describing anisotropic changes in material properties [9, 10].

This paper describes implementation of anisotropic damage mechanics in the material point method (MPM) based on damage tensor approach proposed by Chaboche [6]. In MPM, an object is discretized into a collection of material points [11, 12]. Each particle tracks its state including velocity, stress, strain, and any history-dependent properties such as damage. On each time step, an incremental deformation gradient is applied to each particle to update stresses and strains by the material’s constitutive law. These constitutive laws can be extended to initiate, evolve, and track damage. Because this paper’s derivations involve only constitutive-law steps, the derived MPM methods could also be applied to finite element analysis (FEA) code by altering constitutive laws of materials assigned to each element. The particles in MPM, however, provide convenient options for tracking damage orientation and history [12].

A reader might wonder (as did the authors) why another paper on damage mechanics is needed? This paper developed out of the seemingly straight-forward task of implementing prior damage methods in MPM. The process, however, revealed inconsistencies in prior MPM and FEA methods, especially when claims were made connecting to fracture mechanics. The resolution of such issues led to some highlights, and motivations, for this paper:

1. The damage mechanics here is fully anisotropic in contrast to most models that are based on isotropic damage mechanics. For example, the first use of MPM for damage mechanics [13] was based on isotropic damage mechanics from Oliver [3, 4]. A recent paper used damage field gradients to detect failure surfaces, but also used isotropic damage methods (with mention of future preference to use anisotropic methods) [14].
2. A new “damage strain partitioning tensor” (Δ) is derived as a function of assumed \mathbf{D} . This new tensor simplifies numerical implementation of damage mechanics and demonstrates the connection between anisotropic damage evolution and a physical crack. By finding Δ implied by isotropic damage mechanics, we show that isotropic damage should never be claimed as connected to a crack.
3. A common theme of damage mechanics is to develop methods that can model cracking processes without tracking explicit cracks. A connection between damage mechanics and fracture mechanics is made by relating energy dissipation caused by damage to fracture toughness associated with crack propagation [3, 4], but we are unaware of single-code results that validate this connection. This paper exploits MPM’s ability to handle explicit crack propagation in arbitrary directions [15, 16, 17, 18] to run side-by-side comparisons between anisotropic damage mechanics and explicit fracture mechanics. The two methods can agree, but damage mechanics properties must be calibrated to reflect spread of damage over finite volumes around failure planes.
4. A new stability condition is derived that imposes a spatial resolution requirement as a function of softening law properties.

2. NUMERICAL METHODS

The particles in MPM (or elements in FEA) will start as undamaged but may transition to a damaged state. When damaged, they are modeled as containing a crack spanning the particle's entire cross section. Macroscopic damage zones or cracks are thus represented by a collection of neighboring damaged particles. Clearly the problem must be discretized with sufficient resolution that a collection of damage particles can describe sufficient damage zone detail. Damaged particles partition strain into elastic strain (ϵ_e) and cracking strain (ϵ_c). Elastic strain is strain on the intact portion of the particle. Cracking strains are related to an implied displacement discontinuity within the particle. This implementation considers materials that are small-strain, isotropic materials prior to damage (with E , G , ν , and α for tensile modulus, shear modulus, Poisson's ratio, and thermal expansion coefficient). Once damage initiates, however, the material becomes anisotropic depending on orientation of the damage.

2.1. Assumptions

A complete analysis follows from these assumptions — 1) a failure surface to predict initiation of failure; 2) a form for \mathbf{D} to describe anisotropic response after cracking; and 3) softening laws to describe crack tractions as a function of cracking strains. Because these assumptions are necessary and sufficient, attempts to add additional rules, such as a damage evolution law, would create an inconsistent model. The damage evolution process is an output of the model that is determined by softening laws and obeys thermodynamics conditions for energy dissipation.

All particles start as undamaged and evolve by conventional methods until damage initiates. The first assumption is that failure initiation in an isotropic material can be predicted by a failure surface in principle stress space [13]. When the stress state reaches the surface, failure initiates and the implied crack normal, $\hat{\mathbf{n}}$, is defined by a vector normal to the failure surface (relative to principle stress axes). The normal at initiation is assigned to the particle. The normal remains fixed to the initiated crack plane, but may evolve as the plane shifts due to particle rotation or deformation (in this small-stain implementation (see Appendix II), only particle rotation evolves the normal).

For a concrete failure-surface in isotropic materials, we used a failure surface where a crack initiates when either a maximum principle stress exceeds the material's tensile strength (σ_n) or the maximum shear stress exceeds its shear strength (τ_t). This failure surface (in 2D or 3D) is shown in Fig. 1. When viewed down the $\sigma_1 = \sigma_2 = \sigma_3$ diagonal, the 3D surface is hexagonal rod with point-to-point diagonal equal to τ_t and apex at $\sigma_1 = \sigma_2 = \sigma_3 = \sigma_n$. For tensile failure, the crack normal is along the maximum principle stress direction; for shear failure, it is rotated 45° from the principle stress directions. The use of two strengths are to connect the analysis of opening and shear failure or to tensile (mode I) and shear (modes II and III) fracture mechanics. The dashed line in Fig. 1A is an example of an all alternative criterion, whose choice would require only trivial modifications.

The core of anisotropic damage mechanics is an assumption for \mathbf{D} . A potential \mathbf{D} can be derived by postulating an altered compliance tensor $\tilde{\mathbf{S}}$ for the damaged material. Starting from Eq. (1), the resulting \mathbf{D} is

$$\boldsymbol{\epsilon} = \mathbf{S}_0(\mathbf{I} - \mathbf{D})^{-1}\boldsymbol{\sigma} + \alpha\Delta T = \tilde{\mathbf{S}}\boldsymbol{\sigma} + \alpha\Delta T \quad \text{or} \quad \mathbf{D} = \mathbf{I} - \tilde{\mathbf{S}}^{-1}\mathbf{S}_0 \quad (2)$$

where $\mathbf{S}_0 = \mathbf{C}_0^{-1}$ is compliance tensor of the undamaged material. Using a coordinate system with crack plane normal in the x direction, we adopt a damaged-state compliance proposed by

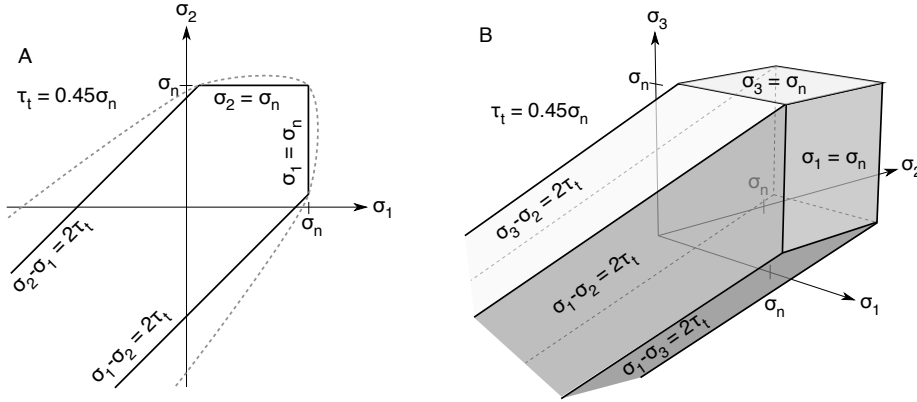


Figure 1. Simple principle stress failure criteria in 2D (A) and 3D (B). Failure initiates when maximum principle stress is positive and reaches σ_n or when any maximum shear stresses reaches τ_t . The two surfaces are for specific example of $\tau_t = 0.45\sigma_n$. The dashed line in A provides an alternative failure surface that could easily be implemented.

Chaboche [8], which leads to:

$$\tilde{\mathbf{S}} = \begin{bmatrix} \frac{1}{(1-d_n^*)E} & -\frac{\nu}{E} & -\frac{\nu}{E} & 0 & 0 & 0 \\ -\frac{\nu}{E} & \frac{1}{E} & -\frac{\nu}{E} & 0 & 0 & 0 \\ -\frac{\nu}{E} & -\frac{\nu}{E} & \frac{1}{E} & 0 & 0 & 0 \\ 0 & 0 & 0 & \frac{1}{G} & 0 & 0 \\ 0 & 0 & 0 & 0 & \frac{1}{(1-d_{xz})G} & 0 \\ 0 & 0 & 0 & 0 & 0 & \frac{1}{(1-d_{xy})G} \end{bmatrix} \quad \text{and} \quad \mathbf{D} = \begin{bmatrix} d_n & 0 & 0 & 0 & 0 & 0 \\ \frac{\nu}{1-\nu}d_n & 0 & 0 & 0 & 0 & 0 \\ \frac{\nu}{1-\nu}d_n & 0 & 0 & 0 & 0 & 0 \\ 0 & 0 & 0 & 0 & 0 & 0 \\ 0 & 0 & 0 & 0 & d_{xz} & 0 \\ 0 & 0 & 0 & 0 & 0 & d_{xy} \end{bmatrix} \quad (3)$$

These matrices are using Voigt form to reduce 4th rank tensors to matrices and stress and strain tensors to vectors: $\boldsymbol{\sigma} = (\sigma_{xx}, \sigma_{yy}, \sigma_{zz}, \tau_{yz}, \tau_{xz}, \tau_{xy})$ and $\boldsymbol{\varepsilon} = (\varepsilon_{xx}, \varepsilon_{yy}, \varepsilon_{zz}, \gamma_{yz}, \gamma_{xz}, \gamma_{xy})$ (note the engineering shear strains). The \mathbf{D} tensor depends on three damage variables d_n , d_{xy} , and d_{xz} where d_n is related to d_n^* by

$$d_n = \frac{d_n^*(1-\nu)}{1-\nu-2(1-d_n^*)\nu^2} \quad (4)$$

In the damaged state, the material becomes an orthotropic material with the evolving nine elastic properties given by $\tilde{E}_{xx} = (1-d_n^*)E$, $\tilde{E}_{yy} = \tilde{E}_{zz} = E$, $\tilde{G}_{xy} = (1-d_{xy})G$, $\tilde{G}_{xz} = (1-d_{xz})G$, $\tilde{G}_{yz} = G$, $\tilde{\nu}_{xy} = \tilde{\nu}_{xz} = (1-d_n^*)\nu$, and $\tilde{\nu}_{yz} = \nu$. Note that d_n^* defines modulus change while d_n defines a compliance element change: $\tilde{C}_{11} = (1-d_n)C_{11}$. The damage parameters range from 0 (undamaged or initial properties) to 1 (failed or zero stiffness normal or tangential to the crack plane). The $\nu/(1-\nu)$ in D_{12} and D_{13} arises because $C_{12} = C_{13} = C_{23} = C_{11}\nu/(1-\nu)$ for an isotropic material. Finally, the thermal expansion coefficients of the damaged material are the same as the initial material and therefore omitted from subsequent equations (although computations should use $\boldsymbol{\varepsilon} - \boldsymbol{\alpha}\Delta T$ in place of $\boldsymbol{\varepsilon}$ to allow for residual strains).

The final assumptions are to propose softening laws for normal traction (T_n) and for two tangential tractions (T_{xy} and T_{xz}) to the crack plane:

$$T_n = \sigma_n f_n(\delta_n), \quad T_{xy} = \tau_t f_t(\delta_{xy}), \quad \text{and} \quad T_{xz} = \tau_t f_t(\delta_{xz}) \quad (5)$$

where $f_n(\delta_n)$ and $f_t(\delta_t)$ are two monotonically decreasing functions with $f_n(0) = f_t(0) = 1$ and δ_n , δ_{xy} , and δ_{xz} are maximum normal and shear cracking strains to be defined later. For an isotropic material, the two shear directions use the same strength (τ_t) and softening law

($f_t(\delta)$), but can be damaged by different amounts (and this changes \tilde{G}_{xy} and \tilde{G}_{xz} by different amounts) as determined by δ_{xy} and δ_{xz} . The areas under these softening laws are connected to tensile and shear energies released by propagation of damage. Note that these softening laws are necessary and sufficient for tracking evolution of d_n , d_{xy} , and d_{xz} . In other words, damage mechanics models cannot have both softening and damage evolution laws — only one is allowed and the second is determined by the first.

In summary, only two material properties are needed — normal and tangential softening laws. Two underlying assumptions are failure surface shape (besides scaling provided by σ_n and τ_t in the softening laws) and the form of \mathbf{D} . The failure surface shape could be revised based on observations of failure in a specific material, which could make that shape a third material property. Its choice has no bearing on the subsequent damage modeling; its only role is to initiate damage and determine the implied crack surface normal vector. The form of \mathbf{D} is crucial to implementation. We assume a three-parameter \mathbf{D} from Chaboche [8] is rational for damage in isotropic materials; some other \mathbf{D} choices are discussed.

2.2. Stress and Strain Updates

Prior to damage initiation, the particles update as a standard isotropic material. This section describes the new updates that are needed after damage initiation. Given a post-initiation strain increment, $d\boldsymbol{\epsilon}$, in displacement-driven MPM code, an update in stress after damage initiation can be written as

$$d\boldsymbol{\sigma} = \mathbf{C}_0 d\boldsymbol{\epsilon} - d(\mathbf{D}\mathbf{C}_0\boldsymbol{\epsilon}) = \mathbf{C}_0 \left(\mathbf{I} - \mathbf{S}_0 \frac{d(\mathbf{D}\mathbf{C}_0\boldsymbol{\epsilon})}{d\boldsymbol{\epsilon}} \right) d\boldsymbol{\epsilon} = \mathbf{C}_0 (\mathbf{I} - \Delta) d\boldsymbol{\epsilon} \quad (6)$$

where $\Delta = \mathbf{S}_0 d(\mathbf{D}\mathbf{C}_0\boldsymbol{\epsilon})/d\boldsymbol{\epsilon}$ is a fourth-rank tensor that is derived from undamaged material properties and \mathbf{D} . To understand Δ and to track damage evolution, we partition input strain into increments in elastic ($d\boldsymbol{\epsilon}_e$) and cracking ($d\boldsymbol{\epsilon}_c$) strain in the crack axis system where $d\boldsymbol{\epsilon} = d\boldsymbol{\epsilon}_e + d\boldsymbol{\epsilon}_c$. Because elastic strain is derived from undamaged properties, the strain partitioning reduces to:

$$d\boldsymbol{\epsilon}_e = \mathbf{S}_0 d\boldsymbol{\sigma} = (\mathbf{I} - \Delta) d\boldsymbol{\epsilon} \quad \text{and} \quad d\boldsymbol{\epsilon}_c = d\boldsymbol{\epsilon} - d\boldsymbol{\epsilon}_e = \Delta d\boldsymbol{\epsilon} \quad (7)$$

Thus Δ is a “damage strain partitioning tensor” that provides the increment in cracking strain caused by an increment in global strain. We are unaware of this tensor being defined in previous damage mechanics models. Its derivation facilitates implementation and interpretation of anisotropic damage mechanics.

For an isotropic material and \mathbf{D} in Eq. (3), we find Δ by first expanding:

$$\mathbf{D}\mathbf{C}_0\boldsymbol{\epsilon} = \left(C_{11}d_n\boldsymbol{\epsilon}_n, \frac{C_{11}\nu}{1-\nu}d_n\boldsymbol{\epsilon}_n, \frac{C_{11}\nu}{1-\nu}d_n\boldsymbol{\epsilon}_n, 0, Gd_{xz}\gamma_{xz}, Gd_{xy}\gamma_{xy} \right) \quad (8)$$

where

$$\boldsymbol{\epsilon}_n = \boldsymbol{\epsilon}_{xx} + \frac{\nu}{1-\nu}(\boldsymbol{\epsilon}_{yy} + \boldsymbol{\epsilon}_{zz}) \quad (9)$$

is an effective strain normal to the crack. Differentiating this vector with respect to strain tensor and pre-multiplying by \mathbf{S}_0 , the only non-zero elements of Δ are:

$$\Delta_{11} = \frac{\partial(d_n\boldsymbol{\epsilon}_n)}{\partial\boldsymbol{\epsilon}_{xx}}, \quad \Delta_{12} = \frac{\partial(d_n\boldsymbol{\epsilon}_n)}{\partial\boldsymbol{\epsilon}_{yy}}, \quad \Delta_{13} = \frac{\partial(d_n\boldsymbol{\epsilon}_n)}{\partial\boldsymbol{\epsilon}_{zz}} \quad (10)$$

$$\Delta_{55} = \frac{\partial(d_{xz}\gamma_{xz})}{\partial\gamma_{xz}}, \quad \Delta_{56} = \frac{\partial(d_{xz}\gamma_{xz})}{\partial\gamma_{xy}}, \quad \Delta_{65} = \frac{\partial(d_{xy}\gamma_{xy})}{\partial\gamma_{xz}}, \quad \text{and} \quad \Delta_{66} = \frac{\partial(d_{xy}\gamma_{xy})}{\partial\gamma_{xy}} \quad (11)$$

Note that Δ describes an anisotropic change in cracking strain and these elements apply to the crack axis system with crack normal, $\hat{\mathbf{n}} = (1, 0, 0)$, in the x direction. The only assumptions in deriving Δ are that $\partial d_n/\partial\gamma_{ij} = \partial d_{xy}/\partial\boldsymbol{\epsilon}_{ii} = \partial d_{xz}/\partial\boldsymbol{\epsilon}_{ii} = 0$, which implies that crack sliding due $d\gamma_{xy}$ or $d\gamma_{xz}$ changes only d_{xy} or d_{xz} , respectively and crack opening due to $d\boldsymbol{\epsilon}_{xx}$, $d\boldsymbol{\epsilon}_{yy}$, or

$d\epsilon_{zz}$ changes only d_n . Physically, this response corresponds to the usual decoupling of tensile and shear modes in fracture mechanics. Finally, this Δ shows that the only cracking strain increments (as full differentials) in the crack axis system are:

$$d\epsilon_{c,xx} = d(d_n \epsilon_n), \quad d\gamma_{c,xy} = d(d_{xy} \gamma_{xy}), \quad \text{and} \quad d\gamma_{c,xz} = d(d_{xz} \gamma_{xz}) \quad (12)$$

2.2.1. Strain Increment with an Elastic Update To detect an elastic update with no damage evolution (or to detect if damage evolution described below is needed), the next task is to look at crack surface tractions. In the crack axis system, the crack traction update is:

$$dT = d\sigma \hat{n} = \mathbf{C}_0(\mathbf{I} - \Delta)d\epsilon \hat{n} = (d\sigma_{xx}, d\tau_{xy}, d\tau_{xz}) \quad (13)$$

$$= (C_{11}(d\epsilon_n - d(d_n \epsilon_n)), G(d\gamma_{xy} - d(d_{xy} \gamma_{xy})), G(d\gamma_{xz} - d(d_{xz} \gamma_{xz}))) \quad (14)$$

We first assume the current update occurs with no damage evolution (*i.e.*, constant d_n , d_{xy} , and d_{xz}) such that $dT^{trial} = (C_{11}(1 - d_n)d\epsilon_n, G(1 - d_{xy})d\gamma_{xy}, G(1 - d_{xz})d\gamma_{xz})$. If tractions, $T + dT^{trial}$ are all below the current strength of the softened material, the update is elastic (*i.e.*, unloading or reloading) and damage variables remain constant. In an elastic update, $\Delta = \mathbf{D}^T$, strains increment by Eq. (7), and stress increment is $d\sigma = \mathbf{C}_0 d\epsilon_e = \mathbf{C}_0(\mathbf{I} - \mathbf{D}^T)d\epsilon = (\mathbf{I} - \mathbf{D})\mathbf{C}_0 d\epsilon$ (by symmetry of \mathbf{C}_0 and \mathbf{DC}_0).

An elastic update of a damaged particle, however, must prevent crack surfaces crossing by keeping ϵ_n nonnegative. Thus if $\epsilon_{c,xx} + d\epsilon_{c,xx} < 0$, the update changes to $d\epsilon_{c,xx} = -\epsilon_{c,xx}$, which stops cracking strain at zero. The stress normal to the crack plane then updates with

$$d\sigma_{xx} = C_{11}(d\epsilon_n - d\epsilon_{c,xx}) = C_{11}(d\epsilon_n + \epsilon_{c,xx}) \quad (15)$$

which corresponds to compressive stress transfer across contacting crack surface as if the material was now undamaged in that direction.

2.2.2. Strain Increment with Damage Evolution If the above trial traction exceeds either the current normal or shear strength, the current strain increment is causing damage. For normal damage evolution (and starting from prior point equal to the current strength), normal traction must track the change in strength given by the normal softening law:

$$dT_n = C_{11}(d\epsilon_n - d(d_n \epsilon_n)) = \sigma_n f'_n(\delta_n) d\delta_n \quad (16)$$

where δ_n is the maximum x direction cracking strain experienced by the particle ($\delta_n = \max(\epsilon_{c,xx})$). During damage loading $\epsilon_{c,xx}$ is at its maximum value and therefore δ_n increments along with $\epsilon_{c,xx}$. From Δ , the increments are $d\delta_n = d\epsilon_{c,xx} = d(d_n \epsilon_n)$. Substituting into Eq. (16) gives

$$\frac{d\delta_n}{d\epsilon_n} = \frac{1}{1 + \epsilon_{n0} f'_n(\delta_n)} \quad \text{with solution} \quad \epsilon_n = \delta_n + \epsilon_{n0} f_n(\delta_n) \quad (17)$$

where $\epsilon_{n0} = \sigma_n / C_{11}$ is the initiation normal strain. At initiation of failure, $\delta_n = 0$, $f_n(0) = 1$, and $\epsilon_n = \epsilon_{n0}$. At failure, $\delta_n = \delta_{n,max}$ (the critical cracking strain), $f_n(\delta_{n,max}) = 0$, and $\epsilon_n = \delta_n = \delta_{n,max}$. In strain driven methods (*i.e.*, both MPM and FEA), δ_n can only change when $d\epsilon_n > 0$ and it can only increase. In other words, stability requires $d\epsilon_n/d\delta_n > 0$ or $-f'(\delta_n) < 1/\epsilon_{n0}$ for all δ_n . The consequences of this requirement are explained below.

During damage evolution, the increment $d\delta_n$ is found from differential equation in Eq. (17) (an analytical solution is possible for linear softening, but numerical methods are needed for non-linear softening). Once $\delta_n \rightarrow \delta_n + d\delta_n$, the normal traction is controlled by the normal softening law and is given by:

$$T_n = (1 - d_n)C_{11}\epsilon_n = \sigma_n f_n(\delta_n) \quad (18)$$

Solving for updated damage variable gives:

$$d_n = 1 - \frac{\epsilon_{n0}}{\epsilon_n} f_n(\delta_n) = \frac{\delta_n}{\delta_n + \epsilon_{n0} f_n(\delta_n)} \quad (19)$$

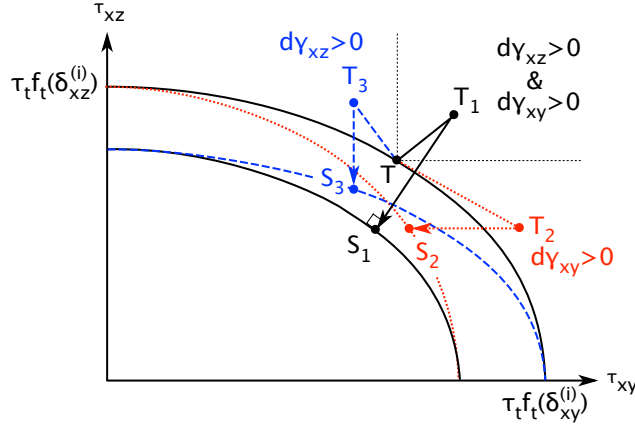


Figure 2. An elliptical failure surface for two shear stresses tangential to the crack plane. T is starting point on current failure surface and T_i are three trial updates outside the failure envelop. After damage evolution, the trial update result to points S_i on one of three updated failure surfaces.

The first form holds only during damage evolution, but the second version holds always by using the current value of δ_n that was incremented during the most recent damage evolution step. Note that computer code does not need to track d_n — it can always be calculated from δ_n , ε_{n0} , and the softening law.

Because initiation of damage provides only a normal vector, the orientation of the x - y and x - z shear planes are arbitrary. For consistency in 3D anisotropic damage processes, evolution of the two shear damage parameters must be considered together by imposing a “current shear strength” failure surface for shear strength tangential to the crack plane. Figure 2 shows an elliptical failure surface where the semi-axes of the ellipse are the current strengths in the x - y and x - z planes due to current damage δ_{xy} and δ_{xz} . The figure also shows an initial state on current failure surface (T) and three trial updates corresponding to three types of damage evolution — T_1 when both $d\gamma_{xy} > 0$ and $d\gamma_{xz} > 0$, T_2 when only $d\gamma_{xy} > 0$, and T_3 , when only $d\gamma_{xz} > 0$. The damage evolution is calculated by finding S_1 , S_2 , or S_3 on the updated failure surface.

For starting point $T = (\tau_{xy}^{(0)}, \tau_{xz}^{(0)})$, the trial points are all $T + dT^{trial}$. The point S_1 is at:

$$S_1 = \left(\tau_{xy}^{(0)} + G_{xy}(d\gamma_{xy} - d\delta_{xy}), \tau_{xz}^{(0)} + G_{xz}(d\gamma_{xz} - d\delta_{xz}) \right) \quad (20)$$

The damage increments, $d\delta_{xy}$ and $d\delta_{xz}$, are found by solving for S_1 on the updated failure surface:

$$\left(\frac{\tau_{xy}^{(0)}/G + d\gamma_{xy} - d\delta_{xy}}{\gamma_{t0}f_t(\delta_{xy} + d\delta_{xy})} \right)^2 + \left(\frac{\tau_{xz}^{(0)}/G + d\gamma_{xz} - d\delta_{xz}}{\gamma_{t0}f_t(\delta_{xz} + d\delta_{xz})} \right)^2 = 1 \quad (21)$$

where $\gamma_{t0} = \tau_t/G$ is the initiation tangential strain. This starting point assumes initial shear stresses are positive. For negative shear stresses, change signs of stresses, strains, and strain increments, apply the following algorithm, and then change the signs back (see Appendix II).

To solve for the two unknowns ($d\delta_{xy}$ and $d\delta_{xz}$), we require the return vector from T_1 to S_1 to be normal to the new failure surface. The return vector is:

$$T_1 - S_1 = G(d\delta_{xy} - d_{xy}d\gamma_{xy}, d\delta_{xz} - d_{xz}d\gamma_{xz}) = G(\gamma_{xy}dd_{xy}, \gamma_{xz}dd_{xz}) \quad (22)$$

Calculating the normal to the updated failure surface and making it normal to $T_1 - S_1$, a second equation becomes

$$\frac{(\tau_{xy}^{(0)}/G + d\gamma_{xy} - d\delta_{xy})(d_{xz}d\gamma_{xz} - d\delta_{xz})}{(\gamma_{t0}f_t(\delta_{xy} + d\delta_{xy}))^2} - \frac{(\tau_{xz}^{(0)}/G + d\gamma_{xz} - d\delta_{xz})(d_{xy}d\gamma_{xy} - d\delta_{xy})}{(\gamma_{t0}f_t(\delta_{xz} + d\delta_{xz}))^2} = 0 \quad (23)$$

These two equations are easily solved by Newton's method in a few steps (and the above forms are scaled well for numerical stability). After updating $\delta_{ij} \rightarrow d\delta_{ij} + d\delta_{ij}$, the cracking strain increments and new damage variables are:

$$d\gamma_{c,ij} = d\delta_{ij} \quad \text{and} \quad d_{ij} = \frac{\delta_{ij}}{\delta_{ij} + \gamma_{t0}f_t(\delta_{ij})} \quad \text{for } ij = xy \text{ and } xz \quad (24)$$

The return vector that is normal to the updated failure surface minimizes the distance from T_1 to that surface, which also minimizes the energy norm. By Eq. (22), the minimum distance corresponds to minimized changes in damage parameters, which, as explained below, minimizes the dissipated energy. It is likely that real softening materials would prefer the minimal energy process.

For trial point T_2 , only $d\gamma_{xy} > 0$ and thus only shear damage in the x - y plane is possible. The return vector to S_2 must be horizontal and $d\delta_{xy}$ is found by solving

$$\left(\frac{\tau_{xy}^{(0)}/G + d\gamma_{xy} - d\delta_{xy}}{\gamma_{t0}f_t(\delta_{xy} + d\delta_{xy})} \right)^2 + \left(\frac{\tau_{xz}^{(trial)}}{\gamma_{t0}f_t(\delta_{xz})} \right)^2 = 1 \quad (25)$$

For linear softening, this equation has an analytical solution. For nonlinear softening, it can be efficiently solved using Newton's method. $\gamma_{c,xy}$ and d_{xy} are found by Eq. (24) while $d\gamma_{c,xz} = d_{xz}d\gamma_{xz}$ because it is an elastic update. The analysis for trial point T_3 is identical but interchanges shear components.

Finally, 2D modeling has only one shear stress – τ_{xy} . It updates by the methods identical to normal direction damage (except no need to check for contact) or by:

$$\frac{d\delta_{xy}}{d\gamma_{xy}} = \frac{1}{1 + \gamma_{t0}f'_t(\delta_{xy})}, \quad d\gamma_{c,xy} = d\delta_{xy}, \quad \delta_{xy} \rightarrow \delta_{xy} + d\delta_{xy}, \quad \text{and} \quad d_{xy} = \frac{\delta_{xy}}{\delta_{xy} + \gamma_{t0}f_t(\delta_{xy})} \quad (26)$$

2.3. Energy Dissipation and Failure

A connection to fracture mechanics follows by evaluating energy dissipation rate, which is

$$d\Omega = \sigma \cdot d\epsilon - d\Psi \quad \text{where} \quad \Psi = \frac{1}{2}(\mathbf{I} - \mathbf{D})\mathbf{C}_0\epsilon \cdot \epsilon \quad (27)$$

is Helmholtz or stored elastic energy (for an isothermal process) and $\mathbf{A} \cdot \mathbf{B}$ is tensor inner product (or dot product of Voigt form vectors). The result is

$$d\Omega = \frac{1}{2}(d\mathbf{D}\mathbf{C}_0)\epsilon \cdot \epsilon = \frac{1}{2}C_{11}\epsilon_n^2 dd_n + \frac{1}{2}G\gamma_{xy}^2 dd_{xy} + \frac{1}{2}G\gamma_{xz}^2 dd_{xz} \geq 0 \quad (28)$$

Using Eqs. (19) and corresponding result for shear terms, energy dissipation during damage evolution reduces to

$$\begin{aligned} d\Omega &= \frac{\sigma_n}{2} \left(f_n(\delta_n) - \epsilon_n f'_n(\delta_n) \frac{d\delta_n}{d\epsilon_n} \right) d\epsilon_n + \frac{\tau_t}{2} \left(f_t(\delta_{xy}) - \gamma_{xy} f'_t(\delta_{xy}) \frac{d\delta_{xy}}{d\gamma_{xy}} \right) d\gamma_{xy} \\ &\quad + \frac{\tau_t}{2} \left(f_t(\delta_{xz}) - \gamma_{xz} f'_t(\delta_{xz}) \frac{d\delta_{xz}}{d\gamma_{xz}} \right) d\gamma_{xz} = \frac{d\bar{G}_I}{d\epsilon_n} d\epsilon_n + \frac{d\bar{G}_{II,1}}{d\gamma_{xy}} d\gamma_{xy} + \frac{d\bar{G}_{II,2}}{d\gamma_{xz}} d\gamma_{xz} \end{aligned} \quad (29)$$

where \bar{G}_I , $\bar{G}_{II,1}$, and $\bar{G}_{II,2}$ are opening and two shear (or mode I and mode II, see below about mode III) dissipation energy rates per unit volume.

Total energy density dissipated by normal crack opening between initiation at ϵ_{n0} and current ϵ_n is

$$\bar{G}_I = \frac{\sigma_n}{2} \int_{\epsilon_{n0}}^{\epsilon_n} \left(f_n(\delta) - \epsilon_n f'_n(\delta) \frac{d\delta}{d\epsilon_n} \right) d\epsilon_n \quad (30)$$

Expressions with corresponding terms gives energy dissipation by crack shearing. Integrating the second term by parts and converting to integral over δ_n leads to:

$$\bar{G}_I = \sigma_n \int_0^{\delta_n} f_n(\delta)(1 + \varepsilon_{n0}f'_n(\delta))d\delta + \frac{\sigma_n \varepsilon_{n0}}{2} - \frac{\sigma_n \varepsilon_n f_n(\delta_n)}{2} = \sigma_n \left(\int_0^{\delta_n} f_n(\delta)d\delta - \frac{\delta_n f_n(\delta_n)}{2} \right) \quad (31)$$

The second term is energy released by elastic unloading from current strength $\sigma_n f_n(\delta_n)$ to zero load over total cracking strain of δ_n . At failure, $f_n(\delta_n) = 0$ leading to the expected result for total energy released up to failure of:

$$\bar{G}_{Ic} = \sigma_n \int_0^{\delta_{n,max}} f_n(\delta)d\delta \quad \text{and} \quad \bar{G}_{II,1c} = \bar{G}_{II,2c} = \bar{G}_{IIc} = \tau_t \int_0^{\delta_{t,max}} f_t(\delta)d\delta \quad (32)$$

where $\delta_{n,max}$ and $\delta_{t,max}$ are δ_n and δ_{xy} or δ_{xz} at failure for mode I and shear modes, respectively. To connect to fracture mechanics energy release rate per unit area, multiply by ratio of particle volume to intersected crack surface area (V_p/A_c — see Appendix II) to get toughness:

$$G_{Ic} = \frac{V_p \sigma_n}{A_c} \int_0^{\delta_{n,max}} f_n(\delta)d\delta \quad \text{and} \quad G_{IIc} = \frac{V_p \tau_t}{A_c} \int_0^{\delta_{t,max}} f_t(\delta)d\delta \quad (33)$$

where G_{Ic} and G_{IIc} are critical mode I and mode II toughnesses. A reasonable mixed-mode failure criterion to model decohesion is to assume failure when:

$$\left(\frac{G_I}{G_{Ic}} \right)^{m_I} + \left(\frac{G_{II,1}}{G_{IIc}} \right)^{m_{II}} + \left(\frac{G_{II,2}}{G_{IIc}} \right)^{m_{II}} = \left(\frac{\bar{G}_I}{\bar{G}_{Ic}} \right)^{m_I} + \left(\frac{\bar{G}_{II,1}}{\bar{G}_{IIc}} \right)^{m_{II}} + \left(\frac{\bar{G}_{II,2}}{\bar{G}_{IIc}} \right)^{m_{II}} = 1 \quad (34)$$

where G_{Ic} , G_{IIc} , m_I and m_{II} are all material failure properties.

The connection of tensile and shear damage to mode I and mode II fracture is rigorous for 2D problems (where $G_{II,2} = 0$). For 3D problems, the shear mode terms combine mode II and mode III fracture. The problem is that mode II and mode III are defined in relation to a 3D crack front. If the crack axis system could be defined with y and z directions normal and tangential to the crack front, respectively, then $G_{II,1}$ would be mode II and $G_{II,2}$ would be mode III. But in MPM damage mechanics, a damaged particle has a complete crack and no information about a crack front. Without that information, mode II and mode III cannot be separated and the shear fracture mechanics terms here labeled as mode II correspond to lumped mode II/III shear damage.

The V_p/A_c factor used to convert \bar{G}_I to G_I also provides for conversion of cracking strains into crack opening displacements. The mode I energy term (and same for shear modes) can be rewritten as:

$$G_{Ic} = \frac{V_p \sigma_n}{A_c} \int_0^{\delta_{n,max}} f_n(\delta)d\delta = \int_0^{u_{n,crit}} F_n(u_n)du_n \quad (35)$$

where $u_n = V_p \delta_n / A_c$ is maximum crack opening displacement, failure occurs at $u_{n,crit} = V_p \delta_{n,max} / A_c$, and $F_n(u_n) = \sigma_n f_n(A_c u_n / V_p)$ is total normal traction in terms of crack opening displacement. Similar relations hold for shear opening displacements. Note that δ_{max} 's are determined by softening laws, but are not inputs to those laws (see Appendix I). For example, δ_{max} determined by linear softening gives the expected results of $u_{n,crit} = 2G_{Ic}/\sigma_n$ and $u_{t,crit} = 2G_{IIc}/\tau_t$.

These relations also define the resolution required for stable softening, which as explained above requires $\max(-f'(\delta_n)) < 1/\varepsilon_{n0}$. Because $V_p/A_c \lesssim \Delta x$ (where Δx is the minimum particle, or FEA element, dimension), the stability condition can be rearranging using Eq. (33) to:

$$\Delta x < \min \left(\eta_n \frac{C_{11} G_c}{\sigma_n^2}, \eta_t \frac{G G_c}{\tau_t^2} \right) = \min \left(\eta_n \left(\frac{K_{Ic}}{\sigma_n} \right)^2, \eta_t \left(\frac{K_{IIc}}{\tau_t} \right)^2 \right) \quad (36)$$

where

$$\frac{1}{\eta_n} = \max(-f'_n(\delta_n)) \int_0^{\delta_{n,max}} f_n(\delta) d\delta \quad \text{and} \quad \frac{1}{\eta_t} = \max(-f'_t(\delta_Y)) \int_0^{\delta_{t,max}} f_t(\delta) d\delta \quad (37)$$

are dimensionless stability factors that depend on softening laws, and K_{Ic} and K_{IIc} are mode I and II critical stress intensity factors. In elastic-plastic fracture mechanics, the square of stress intensity divided by initiation stress describes a plastic zone size [19]; here it is damage zone size. The stability condition for damage mechanics is thus that the particle (or element size) must be on the order (or smaller) than the damage zone size near a crack tip. Simulations of brittle materials (low toughness or high strength) require higher resolution than simulations with ductile materials. This spatial condition is analogous to mesh refinement needed to model of snap-back instabilities with cohesive laws [20]. The addition here is that the required refinement is determined by the η factors, which are easily calculated from the assumed softening law. The η factors are a maximum of 2 for linear softening and therefore lower (requiring higher resolution) for every non-linear law. Some seemingly reasonable softening laws have $\eta \rightarrow 0$, which makes them always unstable (e.g. power-law softening with $n < 1$, see Appendix I). A common practice in numerical damage mechanics is to add artificial damping for stability, but none of the examples below needed damping. We suggest some prior needs for damping were caused by use of softening laws and meshes that do not satisfy the above condition on particle (or element) size.

2.4. Post-Failure Evolution

Once failure is detected (usually by fracture criterion such as in Eq. (34)), the modeling enters a post-failure state. This state can be derived by setting $d_n = d_{xy} = d_{xz} = 1$. All post-failure updates set crack plane stresses to zero: $\sigma_{xx} = \tau_{xz} = \tau_{xy} = 0$ and update remaining stresses by elastic methods. The crack strain will continue to evolve representing further crack opening. The cracking strain update simplifies to:

$$(d\varepsilon_{c,xx}, d\gamma_{c,xz}, d\gamma_{c,xy}) = (\max(d\varepsilon_n, -\varepsilon_{c,xx}), d\gamma_{xz}, d\gamma_{xy}) \quad (38)$$

The $\max()$ function in $d\varepsilon_{c,xx}$ is to prevent crack contact. When contact occurs, the σ_{xx} updates by Eq. (15) instead of being set to zero. This approach is modeling frictionless contact. In principle, shear cracking strains could be used to model crack contact with friction, but that refinement is not considered here.

2.5. Remarks

The previous sections fully describe modeling methods for anisotropic damage mechanics for any input initiation criterion, assumed form of \mathbf{D} , and two input softening laws. A complete numerical algorithm is given in Appendix II. The process defines damage parameters that describe degradation of two mechanical properties (E and G) associated with the initially, isotropic material. Cracking strain updates from Δ lead to cracking strains only in the plane of the crack that correspond to normal and shear crack opening displacements. The areas under the softening laws connect the modeling to fracture mechanics. This section considers some alternatives.

2.5.1. Isotropic Damage Mechanics: Most damage mechanics models use a single, scalar damage parameter, d_I , and assume $\mathbf{D} = d_I \mathbf{I}$. This approach can be evaluated as a special case of the above anisotropic damage mechanics. The damage strain partitioning tensor from $\mathbf{D} = d_I \mathbf{I}$ evaluates to:

$$\Delta_{ij} = \frac{\partial(d_I \varepsilon_i)}{\partial \varepsilon_j} = d_I \delta_{ij} + \varepsilon_i \frac{\partial d_I}{\partial \varepsilon_j} \quad (39)$$

Here ε_i are elements of strain tensor (Voigt form). This tensor implies all components of cracking strain change during damage by $d\varepsilon_{c,i} = d(d_I \varepsilon_i)$. A connection of damage evolution to

fracture mechanics requires consideration of crack surface tractions. Using crack normal from the assumed initiation criterion, crack traction updates in the crack axis system are the same as Eq. (14) except uses only a single damage parameter:

$$\begin{aligned} d\mathbf{T} &= (d\sigma_{xx}, d\tau_{xy}, d\tau_{xz}) \\ &= \left(C_{11}(d\epsilon_n - d(d_I\epsilon_n)), G(d\gamma_{xy} - d(d_I\gamma_{xy})), G(d\gamma_{xz} - d(d_I\gamma_{xz})) \right) \end{aligned} \quad (40)$$

Because only a single damage parameter is used, an isotropic model can track only a single softening process. A logical choice would relate traction magnitude, T_c , to crack opening displacement magnitude:

$$\|\mathbf{T}\| = T_c = \sqrt{\sigma_{xx}^2 + \tau_{xy}^2 + \tau_{xz}^2} \quad \text{and} \quad \beta_c = \sqrt{\epsilon_n^2 + (\gamma_{xy}/2)^2 + (\gamma_{xz}/2)^2} \quad (41)$$

where factors of 2 convert to tensorial shear strain. An increment in damage could be found by numerically solving

$$dT_c = \sigma_I f'_I(\beta_c) d\beta_c \quad (42)$$

whenever traction magnitude exceeds the current strength. Energy dissipation would be

$$d\Omega = \frac{1}{2} \mathbf{C}_0 \boldsymbol{\epsilon} \cdot \boldsymbol{\epsilon} dd_I \quad (43)$$

Perhaps the most serious problem of isotropic damage mechanics is that updating damage based on crack tractions (*i.e.*, use of Eq. (42)) cannot be justified. In isotropic damage, the crack tractions depend only on the three cracking strains that happen to be in the plane of the crack (*c.f.*, Eq. (40)), but isotropic damage affects all strains (from Eq. (39)). In contrast, the crack tractions in anisotropic damage mechanics capture all cracking strains and thus provide sufficient information to evolve the damage state. Isotropic damage mechanics must resort to different or additional evolution methods such as evolution based on tensor invariants (*e.g.*, principal stresses, pressure, or deviatoric stresses). Although feasible, such an approach is not damage mechanics that could be claimed as modeling a physical crack; it would be associative plasticity theory with softening. In summary, although isotropic damage might describe some diffuse (and isotropically distributed) damage state, it cannot model cracks of different orientations and cannot be connected to fracture mechanics. The inability of isotropic damage mechanics to represent a crack makes it difficult to do meaningful comparisons to anisotropic damage mechanics. As a consequence, the “Examples” section below includes only anisotropic damage mechanics simulations.

2.5.2. Alternative Damage Tensors: New damage mechanics models can be derived by making new choices for \mathbf{D} , but for the model to connect to a real crack, the cracking strains should have only non-zero $\epsilon_{c,xx}$, $\gamma_{c,xy}$, and $\gamma_{c,xz}$. This property is best visualized using Δ , which must have all zeros in rows 2, 3, and 4 (in Voigt form). The damage tensor used here satisfies this property, but the isotropic damage tensor does not. Alternative models should be restricted to \mathbf{D} choices that also satisfy this property.

2.5.3. Anisotropic Materials: Extension to anisotropic damage in *anisotropic* materials begins with use of anisotropic \mathbf{C}_0 and a new form for \mathbf{D} . We propose a conjecture that the most general damage tensor for a material in which all elements of \mathbf{C}_0 may be nonzero is:

$$D_{ij} = \frac{C_{ij}d_j}{C_{jj}}, \quad \Delta_{ij} = \frac{\partial(d_i\epsilon_{n,i})}{\partial\epsilon_j}, \quad \epsilon_{n,i} = \sum_j \frac{C_{ij}}{C_{ii}}\epsilon_j, \quad \text{with} \quad d_2 = d_3 = d_4 = 0 \quad (44)$$

(repeated indices not summed). This proposal is based on requirement that \mathbf{DC}_0 must be symmetric and that rows 2, 3, and 4 of Δ must be zero (see previous section). The \mathbf{D} used here is a special case of this conjecture with $d_1 = d_n$, $d_5 = d_{xz}$, and $d_6 = d_{xy}$, and $(\epsilon_{n,1}, \epsilon_{n,5}, \epsilon_{n,6}) = (\epsilon_n, \gamma_{xz}, \gamma_{xy})$. Modeling of anisotropic materials also needs failure initiation criteria that account for anisotropic failure processes and softening laws for each d_i in each distinct failure plane. This problem will be the subject of a future publication.

2.5.4. Multiple Cracking: Consider a simulation loaded until some particles initiate and evolve damage, then unloaded and reloaded in an orthogonal direction. Because the above scheme allows only a single crack in each particle, the new loading may cause stresses in cracked particles parallel to their crack that exceed strength of the material. A potential solution is to allow a second crack and damaged constitutive law of:

$$\sigma = (\mathbf{I} - \mathbf{D}_2) \tilde{\mathbf{C}}(\boldsymbol{\varepsilon} - \alpha \Delta T) = (\mathbf{I} - \mathbf{D}_2)(\mathbf{I} - \mathbf{D}) \mathbf{C}_0(\boldsymbol{\varepsilon} - \alpha \Delta T) \quad (45)$$

In other words, we apply a second damage tensor, \mathbf{D}_2 , to the already damaged material. Because the damage material will be orthotropic, the extension to multiple cracks should be based on more analysis of damage to anisotropic materials. The problem could also be viewed as a more complicated damage tensor of:

$$\mathbf{D}_{tot} = \mathbf{D}_2 + \mathbf{D} - \mathbf{D}_2 \mathbf{D} \quad (46)$$

applied to an isotropic material with damage evolution considering tractions on both crack surface.

3. EXAMPLES

3.1. Simple Tension and Compression

The first example was simple tension on a 40×6 mm bar with elastic properties $E = 1000$ MPa, $\nu = 0.33$, and $\rho = 1000$ kg/m³ and background MPM cell size of 1×1 mm² (particle size 0.5×0.5 mm² or four particles per cell). The bar was pulled in tension at 1 m/sec, which was 0.2% of the material's tensile wave speed. Initiation was controlled by principle stress criterion (see Fig. 1) with $\sigma_n = 30$ MPa and $\tau_t = 20$ MPa. The two softening laws assumed linear softening with $G_{Ic} = G_{IIc} = 10$ kJ/m² and failure assumed $m_I = m_{II} = 1$. Implementation details for linear and other softening laws are given in Appendix I. All results in this paper used linear softening laws and selected cell size for each damage parameters to always maintain stability (by Eq. (36)). Because all particles had the same strength, a single over-stressed particle could dominate the failure mode. To avoid over-stressing due to boundary condition effects, a 4 mm buffer of non-softening material (with otherwise identical properties) was used on each end of the specimen.

Figure 3A shows the “Tensile” stress curve. The failure initiated when stress reached the tensile failure stress of 30 MPa. Despite high toughness ($G_{Ic} = 10$ kJ/m²), once damage in one particle reached $d_n = 1$, a brittle fracture (*i.e.*, fast propagation) occurred in a single line of failed particles across the specimen with crack normal in the loading direction. After failure, the simulation continued stably but the specimen vibrated around zero stress as expected for dynamic response of a cut bar (oscillating stresses not shown). All damaging particles stably softened through to final failure, as can be verified by plotting one particle’s stress *vs.* its crack opening displacement (COD). Such plots (not shown) exactly followed the assumed linear softening law decreasing to zero at the maximum COD of $u_{n,crit} = \delta_{n,max} \Delta x = 2sG_{Ic}(0.5) = 0.667$ mm (see Appendix I for calculation of $\delta_{n,max}$).

From principle stresses in simple tension, the first example failed in tension because $\tau_t > \sigma_n/2$. By choosing a lower τ_t (*e.g.*, $\tau_t = 10$) we induced shear failure instead. The stress strain curve for “Shear” failure is in Fig. 3A. The failure initiates when $\sigma_{app} = 2\tau_t$. After initiation of damage, the specimen failed by stable necking and the crack normal was at 45° to the loading direction. Figure 4A shows the necking process up to just before final failure. A common trick in numerical modeling of necking is to introduce weaker zones or a region with a reduced cross section to initiate necking. In these simulation, no such tricks were needed. A neck formed naturally during shear-initiated failure and developed as a stable deformation process.

Another way to promote shear failure is to load in compression instead of tension. By the failure criterion in Fig. 1, compression loading only allows shear failure. Figure 3A shows a stress strain curve for compression loading of a 30×12 mm² bar with $\tau_t = 15$ MPa. Failure initiated

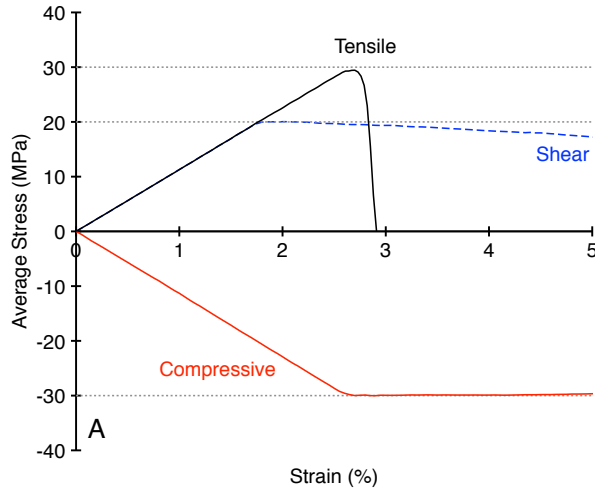


Figure 3. Stress-strain curves for an isotropic material under uniaxial loading in tension or compression. The “Tensile” curve is for $2\tau_t \geq \sigma_n = 30$ MPa, which promotes tensile failure. The “Shear” curve is for $\sigma_n/2 \geq \tau_t = 10$ MPa.

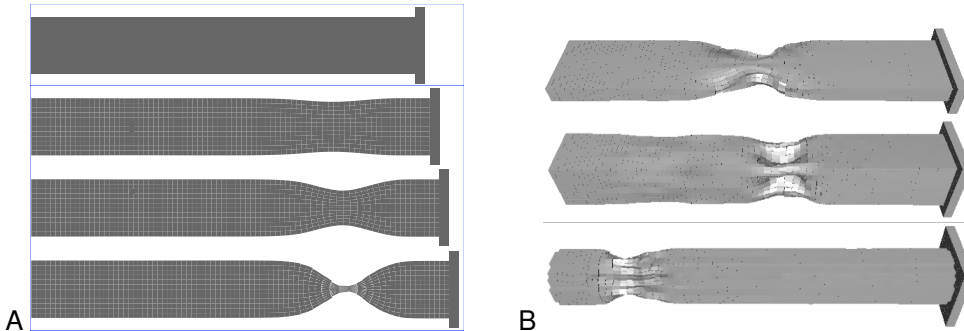


Figure 4. A. The necking process at several stages during uniaxial loading of a material with $\sigma_n/2 \geq \tau_t = 10$ MPa. These relative values induce damage initiation by maximum shear stress at 45° to the loading direction. B. 3D simulations for tensile loading of the same material. The specimens, from top to bottom, had a rectangular, square, or circular cross sections.

when $\sigma_{app} = -2\tau_t$ with damage normal at 45° to the loading direction. Because necking cannot occur in compression, the post failure regime maintained constant stress. By symmetry of the specimen, shear damage propagated in a “X” pattern representing two 45° shear bands across the specimen width. As long as damage remained symmetric, the load remained constant. Eventually numerical effects, which depended on bar aspect ratio, caused one shear band to dominate leading to slippage and a load drop. If specimen symmetry was broken by adding defects or stochastic variations in strength, the failure patterns would be different (see example in Section 3.4).

The results in 3D were very similar, but gave some new information in tensile failure when necking was promoted by low shear strength. Figure 4B shows changes in 3D necking depending on specimen cross section. For an 8×2 mm² rectangular specimen, necking caused thickness reduction across the width, which resembles tensile testing of thin sheets. For 6×6 mm² square and 6 mm diameter cylindrical specimens, the neck was more symmetric. The corners in square specimens caused some additional structure not seen in cylindrical specimens.

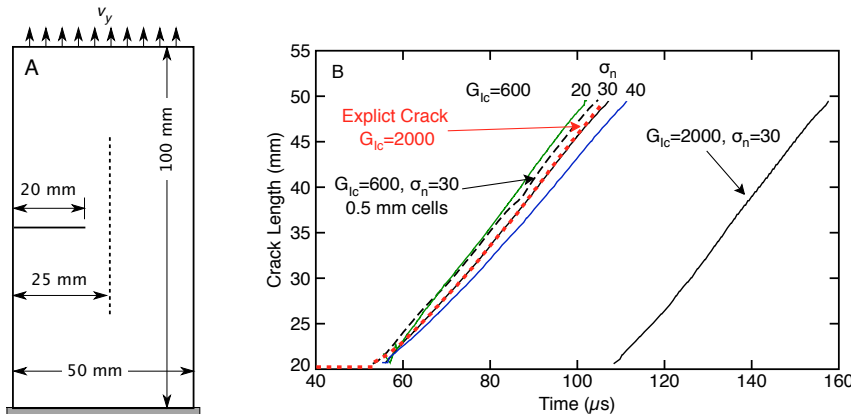


Figure 5. A. Geometry for single edge notched specimen loaded in tension. B. Simulation results for crack length as a function of time. The dotted red curve is MPM simulation with an explicit crack propagation by fracture mechanics. All remaining lines are damage mechanics simulations with two different values for G_{Ic} and three different values for σ_n . The dashed black curve is a damage mechanics simulation at twice the resolution.

3.2. Connection to Fracture Mechanics

One goal of damage mechanics methods is to have an alternative method for modeling crack propagation besides full modeling of explicit cracks. Validation of damage mechanics methods could be tried by comparing its prediction to fracture mechanics experiments on real materials. Unfortunately, few experiments have enough experimental detail for robust comparisons; even with such detail, one cannot be 100% certain that energy release rate is a complete description of real material failure. An alternate approach for validation is to compare damage mechanics predictions to virtual experiments derived by explicit crack modeling in an elastic material with crack propagation determined by crack-tip energy release rate. For example, Fig. 5A shows a single edge notch specimen (with $E = 2500$ MPa, $\nu = 0.33$, and $\rho = 1000$ kg/m³) end loaded at a constant displacement rate of 0.2% the material's tensile wave speed ($v_y = 0.002\sqrt{E/\rho} = 3.16$ m/sec). Figure 5B shows crack (or damage zone) length as a function of time for various material models using an MPM grid cell size of 1 mm. The virtual experiments, or explicit crack model, propagated the crack when $J = G_{Ic}$ where J was calculated using J -integral around the crack tip [17]. By explicit crack methods, the crack initiated at about 54 μ s and propagated at roughly constant crack speed of 600 m/sec² (see dotted red curve in Fig. 5B)

Damage mechanics simulations had the same initial (and explicit) crack, but attempted to model crack propagation as a damage process. First, G_{Ic} was set to same 2000 J/m², mode I strength was guessed as $\sigma_n = 30$ MPa, and softening law was linear (for this pure mode I example, τ_t , G_{IIc} , m_I and m_{II} were not needed). Initiation of crack growth (as measured by particles failing with $d_n \rightarrow 1$), was significantly delayed to about 110 μ s, although the subsequent crack growth rate was similar. This initiation discrepancy was resolved by noting that damaged particles did not develop as a single row of particles along the crack, but rather spread to a damage zone of finite width on both sides of the crack plane. For damage mechanics materials to match fracture mechanics models, one must scale toughness of the damage mechanics materials to account for damage zone size. Here using half the toughness was close, but was still too high because some damage spread more than one particle from the crack plane. By varying toughness, we found that setting toughness to $0.3G_{Ic}$ (or to 600 J/m²) gave a damage mechanics simulation nearly identical to the explicit fracture mechanics simulation (see Fig 5B). Their equivalence is emphasized by comparison of stress states at fixed time of 77 μ s as plotted in Fig 6A and 6B.

But hows does one select the strength property, σ_n , especially when the underlying material used in the fracture mechanics "experiments" was a virtual material with no defined strength

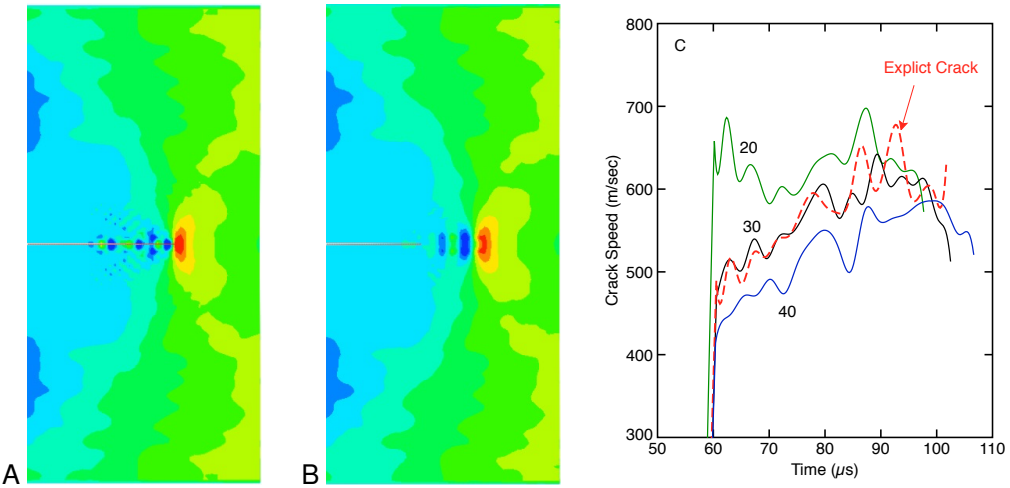


Figure 6. The axial stress distribution at 77 μ s (and after some crack propagation) for A. Explicit crack modeling and B. Damage mechanics modeling. C. Crack growth rate by explicit crack modeling and by damage mechanics modeling using three different values for σ_n .

property? Figure 5B shows simulations with scaled toughness of $G_{Ic} = 600 \text{ J/m}^2$ and σ_n of 20 (green), 30 (black), and 40 (blue) MPa. The tensile strength had very little effect on initiation of failure, but did affect crack propagation speed. Figure 6C shows crack velocity as a function of time for the three strengths (found by smoothing and then differentiating crack length results). Results with $\sigma_n = 30 \text{ MPa}$ gave excellent match to explicit crack results, while $\sigma_n = 20 \text{ MPa}$ and 40 MPa gave crack velocity that was too high or too low, respectively.

These results show that a damage mechanics material can quantitatively match fracture mechanics modeling of an explicit crack, but toughness of the damage mechanics material properties must be scaled down to account for volume of the damaged zone. The strength property may need to be an effective strength chosen to match fracture mechanics, and possibly differing from a material's tensile strength. For example, one specific value ($\sigma_n = 30 \text{ MPa}$) gave best match here even though this virtual material had no tensile strength property. These observations apply to both MPM and FEA damage mechanics models. In other words, all damage mechanics models intended to match fracture predictions must use *apparent* strength and toughness rather than simply choosing measured strength and toughness. Correspondence between fracture mechanics and damage mechanics as well as the meaning and convergence of damage mechanics parameters will be the subject of a future publication.

The energy dissipation calculations in this implementation are independent of mesh size by scaling the toughness/softening law relation in Eq. (33), where V_p/A_c will be close to the particle length. But mesh-independent energy calculations do not imply convergence of damage mechanics models to fracture mechanics models. Figure 5B shows a damage mechanics simulation at twice the resolution (or 0.5 mm cells in dashed black curve). Explicit crack analyses gave identical results at both resolutions (*i.e.*, the explicit crack result in Fig. 5B is a converged result). Although damage mechanics results are slightly shifted at higher resolution, that shift can be explained by better resolution of the damage zone and less spread of dissipated energy to particles away from the crack plane. The higher resolution results can be made to match fracture mechanics well by rescaling G_{Ic} to 750 J/m^2 . Because damage mechanics models result in a damage zone of finite thickness, they will never converge to a zero-thickness crack plane (except in limit of zero thickness particles). Prior claims that damage mechanics is equivalent to fracture mechanics of a crack plane are missing this issue. But damage mechanics can get close to explicit crack modeling by using *apparent* strength and toughness. Perhaps lack of damage zone thickness convergence is an advantage? Explicit crack fracture mechanics is idealizing failure as confined to a 2D plane. Real materials likely develop damage around the plane.

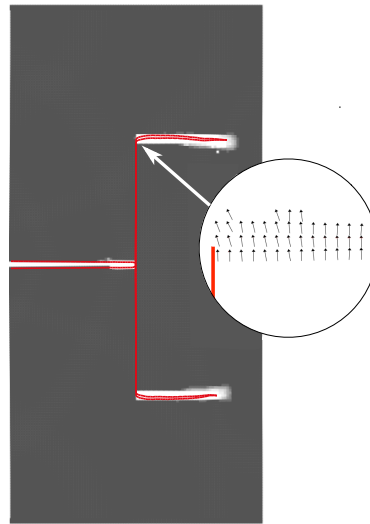


Figure 7. Crack propagation for two interacting cracks. The solid red lines show predictions using explicit crack modeling and fracture mechanics. The white zones show predictions using anisotropic damage mechanics modeling. The inset shows the crack normals near the tip at the top of the vertical crack that were predicted in damage mechanics modeling.

Anisotropic damage mechanics has the potential to model crack-plane discontinuity along with finite thickness damage zones around the crack plane.

A potential application of damage mechanics is to handle crack propagation in problems where explicit crack propagation becomes challenging, such as problems with interacting cracks. The proposed approach is to explicitly model all initial cracks by standard crack methods (an explicit crack in MPM [21] or by discretizing cracks within a FEA mesh). These explicit cracks will create stress concentrations at crack tips and hopefully damage mechanics models will result in damage propagation that matches explicit crack propagation. For example, the dashed, vertical line in Fig. 5A shows a second crack perpendicular to the edge crack. Figure 7 compares propagation of damage by damage mechanics (white zones) to propagation by explicit fracture mechanics of interacting cracks (red lines). The damage mechanics simulation used the scaled material from above and added $\tau_t = \sigma_n$, $G_{Ic} = G_{Ic}$, and $m_I = m_{II} = 1$ to handle mixed mode conditions on the vertical crack. The explicit interacting crack model is described in Ref. [21]. Failure initiated at the edge crack. This crack propagated by pure mode I fracture, but was arrested when it intersected the vertical crack. After a delay, both crack tips of the second crack propagated at right angles to the crack tips. These cracks experienced mixed-mode stress state. The inset shows crack normals developed by damage mechanics. These failures were calculated by the principle stress criterion showing that maximum principle stress was parallel to the crack. For mixed-mode failure predictions, the explicit crack model [21] used the maximum hoop stress criterion [22]. Damage mechanics modeling based on principle stresses reproduced this common mixed-mode failure criterion (*i.e.*, damage initiation showed that the maximum principle stress direction at the vertical cracks was parallel to that crack resulting in perpendicular crack growth).

3.3. Microcracking

Another reason for developing damage mechanics is for problems that require prediction of fracture initiation. Most fracture mechanics approaches deal with an existing crack that grows. In contrast, damage mechanics, at least in principle, has mechanisms both to initiate and propagate damage. This section looks at the phenomenon of layer microcracking. When one layer of a multilayered structure is more brittle than other layers, tensile loading parallel to the layers is often characterized by periodic cracking confined to the brittle layer. Such microcracking

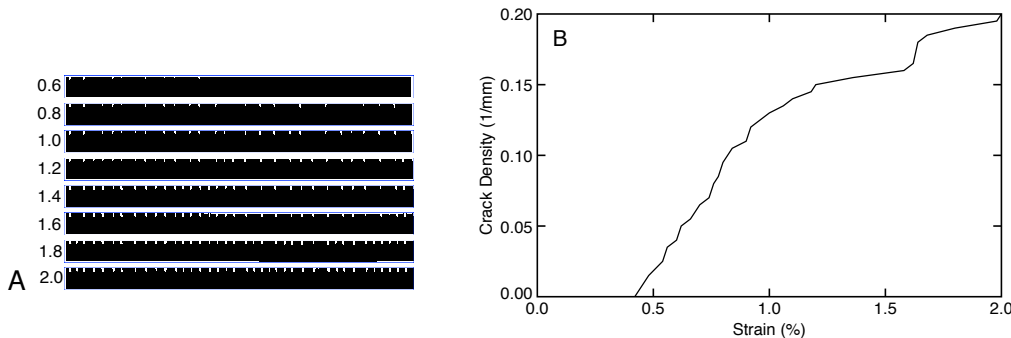


Figure 8. A. Microcracks in the coating layer as a function of applied strain (indicated on the left in %).
B The simulated crack density as a function of applied strain.

(or transverse cracking) can be seen in brittle coatings on polymers [23, 24, 25, 26], in 90° layers of aerospace composites [27, 28], and in all layers of cross-laminated timber [29]. A common experiment to characterize such cracks is to load in tension and observe crack density as a function of applied strain [25, 26]. The typical response is initiation of cracking at some onset strain followed by a rapid increase in crack density, and then by slowing down of cracking that approaches a saturation damage state with periodic microcracks. The damage mechanics method described here can reproduce all these features.

Figure 8A shows snapshots of microcracking in a 2 mm thick brittle coating on a 10 mm thick softer substrate. The coating properties were $E_c = 10,000$ MPa, $\nu_c = 0.33$, and $\rho_c = 1$ g/cm³. Its mode I damage properties were $\sigma_n = 10$ MPa and $G_{Ic} = 100$ J/m³ (shear strength was set high to avoid unrealistic shear failures near boundary conditions and to focus on tensile failure of the brittle layer). The substrate properties were $E_s = 1,000$ MPa, $\nu_s = 0.33$, and $\rho_s = 1$ g/cm³. The 200 mm long sample was pulled at 4 m/sec (which was 0.4% of the substrate material's tensile wave speed). The background MPM grid had 1×1 mm² cells (0.5×0.5 mm² particles). The crack onset strain was 0.44%. All cracks initiated on the surface, propagated to the interface, and then arrested. As strain increased the surface layer developed a periodic cracking pattern (see Fig. 8A). Figure 8B shows simulated crack density as a function of applied strain. Both the periodic cracks and the crack density curve resemble actual experiments on cracking of surface layers [25, 26, 23].

The ability of a damage mechanics model to emulate real-world microcracking means the method has potential for developing new insights into multilayer cracking. Fracture mechanics models are available for predicting 2D cracking of a single, linear elastic layer on a linear elastic substrate [24]. The potential applications of damage mechanics could include cracking of multiple brittle layers, effects of inelastic substrates, or 3D cracking in biaxially loaded films [30, 31].

Note that these simulations used a recently-developed MPM method, called XPIC(m) (of order m), that can remove noise without overdamping [32]. We found that using XPIC(5) gave better microcracking simulations than using standard MPM. While standard MPM became unstable at about 1.75% strain at a prior crack, XPIC(5) simulations remained stable to the end. We suggest that XPIC(m) should be an important component of MPM damage mechanics simulations.

3.4. Stochastic Model

Our final example revisited simple compression from Section 3.1, but instead of assuming all particles have the same strength, the strengths were randomly assigned. In damage mechanics modeling, the use of identical strength particles can result in load situations (such as uniform loading) where all particles approach failure simultaneously or can result in simulations susceptible to boundary condition artifacts. A switch to random strengths creates weak zones that can initiate and perhaps more stably propagate damage. Random strengths are also a better

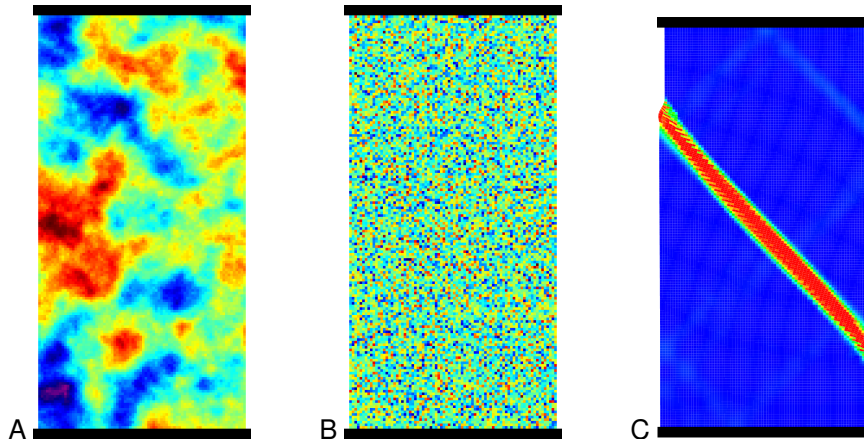


Figure 9. Examples of an elastic block with resolution of 0.25 mm per grid cell. A. Example of GRF distribution of properties. B. Example of uncorrelated Gaussian distribution of properties. C. Example of a failed block. Colored by cracking strain.

model of real materials that have variations in strength throughout their domain. A stochastic damage mechanics model needs Monte Carlo methods: 1. generate numerical models with random strengths; 2. run damage mechanics calculations observing failure and damage process; and 3. repeat on multiple specimens to evaluate mean strength, variations in strength, and types of failure modes.

One approach to stochastic modeling assumes a strength property P has a Gaussian probability distribution $P(x) \sim N(\mu, \sigma)$ with mean μ and standard deviation σ and randomly assigns P to each particle. This approach leads to situations where two locations near each other are uncorrelated or that a very strong particle is adjacent to a very weak particle. Such a model is likely an unrealistic description of real materials. To better model a stochastically varying continuum, we used a Gaussian random field (GRF) [33] rather than randomly assigned strengths. A GRF models a property P that maintains the same overall distribution ($P(x) \sim N(\mu, \sigma)$) but adds a spatial correlation and is widely used in stochastic modeling [33]. For any two points in space, x_i and x_j , the properties $P(x_i)$ and $P(x_j)$ are jointly Gaussian distributed with a correlation based on the distance between them: $\text{Corr}(P(x_i), P(x_j)) = C(d)$ where $d = \|x_i - x_j\|$.

We ran two sets of Monte Carlo numerical experiments for compression of a $10 \times 20 \text{ mm}^2$ block. The first set used a GRF with correlation function $C(d) = e^{-\alpha d^{1.5}}$ and spatial scale parameter $\alpha = 2/3 \text{ mm}^{-1}$. The second set used uncorrelated, randomly assigned strengths (which correspond to $\alpha \rightarrow \infty$). The GRF fields were generated in R [34] using the *RandomFields* package [35]. Four different resolutions were run with grid size of 0.5 mm, 0.25 mm, 0.125 mm and 0.0625 mm. A sample realization for a GRF with grid size of 0.25 mm is plotted in Figure 9A vs. an uncorrelated sample in Fig. 9B. The GRF sample has regions of high or low strength while the uncorrelated sample is a speckle pattern of strengths. The block had mean fixed properties $\nu = 0.3$ and $\rho = 1000 \text{ kg/cm}^3$ and variable properties with mean values of $E = 1 \text{ GPa}$, $\sigma_n = 10 \text{ MPa}$, $\tau_t = 4.5 \text{ MPa}$, $G_{Ic} = 500 \text{ J/m}^2$, and $G_{IIc} = 1000 \text{ J/m}^2$. These variable properties $P = \{E, \sigma_n, \tau_t, G_{Ic}, G_{IIc}\}$ at each material point all were scaled by factor s with normal distribution $s \sim N(1, 0.1)$. We ran 200 simulations for each set and each resolution for a total of 1600 simulations using XPIC(5) for improved stability.

A typical compression failure is shown in Figure 9C. As commonly observed in axial compression in specimens with a sufficiently low aspect ratio to prevent buckling, the specimens failed by a shear band at 45° to the loading direction. Among all replicated specimens, shear bands occurred randomly at $\pm 45^\circ$. If a shear band initiated close to one end, the band would reflect off the end in a V-shaped band. Analogous to the fracture simulations, the thickness of

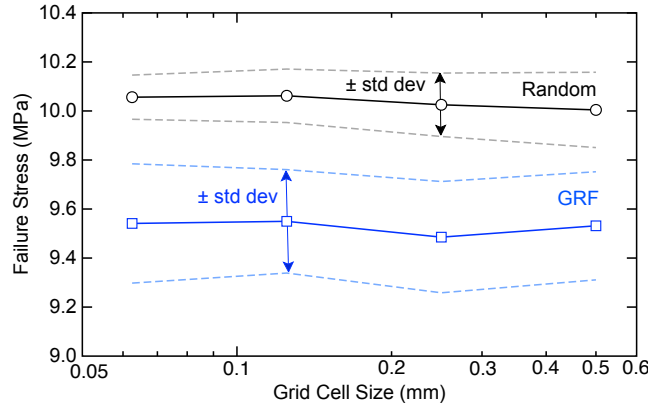


Figure 10. The mean and variance for uncorrelated and GRF specimens as a function of mesh size. The dashed lines indicate ± 1 standard deviation from the mean.

the shear band got thinner for higher resolutions. It is modeling a shear crack and a crack plane is represented more accurately at higher resolution with a thinner damage zone. Despite changes in damage zones, the mean strengths for each set were independent of mesh size (see Fig. 10). This result confirms the mesh scaling term V_p/A_c needed to connect material toughness (G_{Ic} and G_{IIc}) to maximum cracking strains ($\delta_{n,max}$ and $\delta_{t,max}$) correctly scales particle properties for mesh independence. Even though the two sets had the same input normal distribution in properties, the mean strengths were considerably different. The GRF simulations consistently failed at a lower loading stress. In other words, spatial correlation affects strength and therefore should be part of stochastic modeling. The strength is a maximum for uncorrelated strengths ($\alpha \rightarrow \infty$) and decreases for smaller α . A smaller α results in larger defects that can initiate failure. The variance in the results also depended on α . For GRF simulations, the variance is higher and is independent of mesh size. For uncorrelated strengths, the variance is smaller and seems to converge toward zero along with grid cell size. In other words, GRF methods are needed to get mesh independence of both mean and variance. The need to have spatial correlations for mesh independence is similar to MPM plasticity modeling of compression failure by Burghardt *et al.* [36]. They needed non-local plasticity (i.e., a spatial connection in yield response) to get mesh independence of shear failure.

An overlay of stress-strain curves for all uncorrelated and GRF specimens run at the highest resolution (0.0625 mm cells) is given in Fig. 11 (200 curves each). The uncorrelated results (red curves) have higher peak strength and lower variability. The GRF results (black curves) have lower strength and greater variability. The post-failure response for all resolutions was similar at first with a slow decrease from peak strength. Eventually, the initial shear bands propagated into diffuse damage throughout the specimen, which caused a large drop in load. This diffuse damage state happened sooner at low resolution than at high resolution. By comparing variability in simulated stress-strain curves to experimental curves, it might be possible to characterize spatial variations of real materials. One example could be to evaluate properties of timber compared to laminated veneer lumber (LVL). LVL is made by cutting veneer layers from lumber and then gluing them back together with wood grain direction of all layers in the same direction. Experimental work shows that LVL can have better properties than the original timber and lower variability. These differences are qualitatively attributed to distribution of large defects in timber (e.g., knots) compared to randomly dispersed defects in LVL. Monte Carlo simulations using GRFs with different spatial correlations in comparison to experimental stress-strain curves might provide a more quantitative analysis of timber vs. LVL.

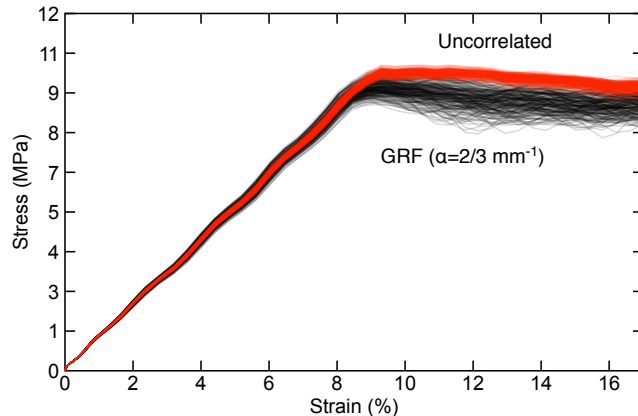


Figure 11. An overlay of all stress strain curves for uncorrelated specimens (red curves) and for GRF specimens (black curves).

4. CONCLUSIONS

We described a full approach to numerical implementation anisotropic damage mechanics through constitutive law phase of any numerical method. Anisotropic damage mechanics is a relatively straight-forward extension of linear elasticity, with the main requirements being to connect damage to cracks and to use softening laws to evolve damage parameters. Two key features of this new implementation were derivation of a new damage strain partitioning tensor, Δ , and definition of spatial resolution required for stability, $\Delta x < \eta(K/\sigma)^2$. The new tensor, which can be derived from any assumed anisotropic damage tensor (or \mathbf{D}), solves the numerical task of partitioning input global strain increment into elastic strains and cracking strains and provides a path to tracking damage evolution from assumed normal and shear traction softening laws. An important observation is that only rows 1, 5, and 6 of Δ have nonzero values, which shows that cracking strains are limited to strains that are physically connected to normal and shear opening displacements of an implied crack. The new spatial resolution requirement may explain why same prior damage mechanics models needed artificial damping for acceptable results while the new results here did not need stabilization.

By evaluating dissipated energy, softening laws and cracking strains can be directly related to normal and shear, or mode I and lumped mode II/III, fracture. Some examples using MPM demonstrated features of the implemented damage mechanics. The fracture examples, in particular, show that anisotropic damage mechanics can reproduce many features of explicit crack modeling using fracture mechanics provided damage material properties are calibrated *apparent* properties. In contrast, we showed that isotropic damage mechanics based on a single scalar damage parameter, d_I , cannot connect to a crack and therefore cannot reproduce explicit crack predictions.

ACKNOWLEDGEMENTS

This work was supported by the National Institute of Food and Agriculture (NIFA) award #2013-34638-21483, of the United States Department of Agriculture (USDA).

5. REFERENCES

REFERENCES

1. Kachanov L. Time of rupture process under creep conditions. *Izv. Akad. Nauk SSR, Otd. Tekh. Nauk* 1958; **8**:26–31.
2. Talreja R. Damage characterization by internal variables. *Damage Mechanics of Composite Materials*, Talreja R (ed.). Elsevier, Amsterdam, 1994; 53–78.
3. Oliver J. Modelling strong discontinuities in solid mechanics via strain softening constitutive equations. Part 2: Numerical simulation. *International Journal for Numerical Methods in Engineering* 1996; **39**(21):3601–3623.
4. Oliver J. Modelling strong discontinuities in solid mechanics via strain softening constitutive equations. Part 1: Fundamentals. *International Journal for Numerical Methods in Engineering* 1996; **39**(21):3575–3600.
5. Ju JW. Isotropic and anisotropic damage variables in continuum damage mechanics. *Journal of Engineering Mechanics* 1990; **116**(12):2764–2770.
6. Chaboche JL. Development of continuum damage mechanics for elastic solids sustaining anisotropic and unilateral damage. *International Journal of Damage Mechanics* 1993; **2**(4):311–329.
7. Chaboche J. Anisotropic creep damage in the framework of continuum damage mechanics. *Nuclear Engineering and Design* 1984; **79**(3):309 – 319.
8. Chaboche J. Le concept de contrainte effective appliquée à l'élasticité et à la viscoplasticité en présence d'un endommagement anisotrope. *Mechanical Behavior of Anisotropic Solids / Comportement Mécanique des Solides Anisotropes*, Boehler JP (ed.). Springer Netherlands, 1979; 737–760.
9. Ladèze P, Lubineau G. An enhanced mesomodel for laminates based on micromechanics. *Comp. Sci & Tech.* 2002; **62**:533–541.
10. Ladèze P, Lubineau G. On a damage mesomodel for laminates: Micro-meso relationships, possibilities, and limits. *Comp Sci & Tech.* 2001; **61**:2149–2158.
11. Bardenhagen SG. Energy conservation error in the material point method. *J. Comp. Phys.* 2002; **180**:383–403.
12. Sulsky D, Chen Z, Schreyer HL. A particle method for history-dependent materials. *Comput. Methods Appl. Mech. Engrg.* 1994; **118**:179–186.
13. Schreyer H, Sulsky D, Zhou SJ. Modeling delamination as a strong discontinuity with the material point method. *Computer Methods in Applied Mechanics and Engineering* 2002; **191**(23–24):2483 – 2507.
14. Homel M, Herbold EB. Field-gradient partitioning for fracture and frictional contact in the material point method. *Int. J. for Numerical Methods in Engineering* 2016; **109**(7):1013–1044.
15. Guo YJ, Nairn JA. Simulation of dynamic 3D crack propagation within the material point method. *Computer Modeling in Engineering & Sciences* 2016; :submitted.
16. Guo Y, Nairn JA. Three-dimensional dynamic fracture analysis in the material point method. *Computer Modeling in Engineering & Sciences* 2006; **16**:141–156.
17. Guo Y, Nairn JA. Calculation of J-integral and stress intensity factors using the material point method. *Computer Modeling in Engineering & Sciences* 2004; **6**:295–308.
18. Nairn JA. Material point method calculations with explicit cracks. *Computer Modeling in Engineering & Sciences* 2003; **4**:649–664.
19. Williams JG. *Fracture Mechanics of Polymers*. John Wiley & Sons, New York, 1984.
20. Carpinteri A. Softening and snap-back instability in cohesive solids. *Int. J. for Numerical Methods in Engineering* 1989; **28**:1521–1527.
21. Nairn JA, Aimeye Y. Modeling interacting and propagating cracks in the material point method: Application to simulation of hydraulic fractures interacting with natural fractures 2016. In preparation.
22. Erdogan F, Sih GC. On the crack extension in plates under plane loading and transverse shear. *Journal of Basic Engineering, ASME* 1963; **85**:519–527.
23. Kim SR, Nairn JA. Fracture mechanics analysis of coating/substrate systems subjected to tension or bending loads II: Experiments in bending. *Engr. Fract. Mech.* 2000; **65**:595–607.
24. Kim SR, Nairn JA. Fracture mechanics analysis of coating/substrate systems subjected to tension or bending loads I: Theory. *Engr. Fract. Mech.* 2000; **65**:573–593.
25. Leterrier Y, Boogh L, Andersons J, Månsen JAE. Adhesion of silicon oxide layers on poly(ethylene terephthalate). I: Effect of substrate properties on coating's fragmentation process. *J. Polym. Sci., Part B: Polymer Physics* 1997; **35**:1449–1461.
26. Leterrier Y, Andersons J, Pitton Y, Månsen JAE. Adhesion of silicon oxide layers on poly(ethylene terephthalate). II. effect of coating thickness on adhesive and cohesive strengths. *J. Polym. Sci., Part B: Polymer Physics* 1997; **35**:1463–1472.
27. Nairn JA. Matrix microcracking in composites. *Comprehensive Composite Materials*, vol. 2, Talreja R, Månsen JAE (eds.). Elsevier Science, 2000; 403–432.
28. Nairn JA, Hu S. Micromechanics of damage: A case study of matrix microcracking. *Damage Mechanics of Composite Materials*, Talreja R (ed.). Elsevier, Amsterdam, 1994; 187–243.
29. Nairn JA. Mechanical properties of cross-laminated timber accounting for non-bonded edges and additional cracks. *European Journal of Wood and Wood Products* 2017; :in press.
30. Leterrier Y, Waller J, Manson JA, Nairn J. Models for saturation damage state in multilayer coatings. *Mechanics of Materials* 2009; **42**:326–334.
31. Leterrier Y, Fischer C, Médico L, Demarco F, Månsen JAE, Bouten P DeGoede J, Nairn JA. Mechanical properties of transparent functional thin films for flexible displays. *Proc. 46th Ann. Tech. Conf. Soc. Vacuum Coaters*, San Francisco, California, May 3-8, 2003.
32. Hammerquist C, Nairn JA. A new method for material point method particle updates that reduces noise and enhances stability. *Computer Methods in Applied Mechanics and Engineering* 2017; :in press.
33. Abrahamsen P. *A review of Gaussian random fields and correlation functions*. Norsk Regnesentral/Norwegian Computing Center, 1997.
34. R Core Team. R: A language and environment for statistical computing, <https://www.R-project.org/>. R Foundation for Statistical Computing, Vienna, Austria 2016.

35. Schlather M, Malinowski A, Menck PJ, Oesting M, Strokor K. Analysis, simulation and prediction of multivariate random fields with package RandomFields. *Journal of Statistical Software* 2015; **63**(8):1–25.
36. Burghardt J, Brannon R, Guilkey J. A nonlocal plasticity formulation for the material point method. *Comput. Methods Appl. Mech. Engrg.* 2012; **225–228**:55–64.

APPENDIX I

Traction during softening is given by $\sigma f(\delta)$ where $f(\delta)$ is a normalized softening law. A coding class to handle any law only needs to provide $f(\delta)$, \bar{G}_c/σ , $f'(\delta)$, and $\max(-f'(\delta))$ (for stability confirmation). These terms depend on σ and G_c (and maybe other parameters). The critical strain for failure, δ_{max} , is not an independent variable because it can be found from Eq. (33) using G_c and a scaling factor $s = A_c/(V_p \sigma)$, where A_c/V_p is calculated once per particle when failure initiates.

For power-law softening, $f(\delta) = 1 - (\delta/\delta_{max})^n$ where $n \geq 1$ and $\delta_{max} = (1+n)sG_c/n$. Code implementation also needs:

$$\frac{\bar{G}(\delta)}{\sigma} = \frac{\delta}{2} \left(1 - \frac{1-n}{1+n} \left(\frac{\delta}{\delta_{max}} \right)^n \right), \quad f'(\delta) = -\frac{n}{\delta_{max}} \left(\frac{\delta}{\delta_{max}} \right)^{n-1},$$

and $\max(-f'(\delta, s)) = \frac{n}{\delta_{max}}$ for $n \geq 1$ or ∞ for $n < 1$

(47)

Note that power law softening with $n < 1$ is always unstable due to $\max(-f'(\delta)) = -f'(0) \rightarrow \infty$. A useful special case is linear softening with $n = 1$ where code implementation is

$$\delta_{max} = 2sG_c, \quad f(\delta) = 1 - \frac{\delta}{\delta_{max}}, \quad \frac{\bar{G}(\delta)}{\sigma} = \frac{\delta}{2}, \quad f'(\delta) = -\frac{1}{\delta_{max}}, \quad \text{and } \max(-f'(\delta)) = \frac{1}{\delta_{max}} \quad (48)$$

For exponential softening $f(\delta) = e^{-k\delta}$ with $\delta_{max} = \infty$ but $k = 1/(sG_c)$. Code implementation also needs:

$$\frac{\bar{G}(\delta)}{\sigma} = \frac{1}{k} - e^{-k\delta} \left(\frac{1}{k} + \frac{\delta}{2} \right), \quad f'(\delta) = -ke^{-k\delta}, \quad \text{and } \max(-f'(\delta, s)) = k \quad (49)$$

Note that among all softening laws enclosing the same area (or the same G_c), a linear softening law minimizes $\max(-f'(\delta, s))$, which makes linear softening the most stable of all laws.

APPENDIX II

This section outlines an algorithm for implementation of 3D anisotropic damage mechanics in an isotropic material; this description is written for MPM particles but could be used for constitutive law phase of any numerical method. Each particle tracks total deformation gradient ($\mathbf{F}^{(p)}$), stress ($\boldsymbol{\sigma}^{(p)}$), cracking strain ($\boldsymbol{\epsilon}_c^{(p)}$), and damage orientation (to allow rotation to the crack axis system), and maximum cracking strains ($\delta_n^{(p)}$, $\delta_{xy}^{(p)}$ and $\delta_{xz}^{(p)}$). Tensors are tracked in global coordinates because MPM force calculations need global coordinate stresses. The damage parameters (d_n , d_{xy} , and d_{xz}) can be tracked or calculated whenever needed (e.g., Eq. (19)).

Each step begins with an imposed displacement gradient, $\nabla \mathbf{u}$, which is equal to $\nabla \mathbf{v} \Delta t$ in dynamic codes where \mathbf{u} is displacement, \mathbf{v} is velocity, and Δt is the time step. First, find incremental deformation gradient, $d\mathbf{F}$, and update the particle's total deformation gradient:

$$d\mathbf{F} = \exp(\nabla \mathbf{u}) \quad \text{and} \quad \mathbf{F}_n^{(p)} = d\mathbf{F} \mathbf{F}_{n-1}^{(p)} \quad (50)$$

The incremental deformation gradient can be approximated by $d\mathbf{F} = \mathbf{I} + \nabla \mathbf{u}$ or efficiently expanded to more terms using the Cayley-Hamilton theorem. Incremental small strain in the initial axis system is $d\boldsymbol{\epsilon} = \mathbf{U}_n^{(p)} - \mathbf{U}_{n-1}^{(p)}$, where $\mathbf{U}_n^{(p)}$ and $\mathbf{U}_{n-1}^{(p)}$ can be found by polar decomposition of $\mathbf{F}_n^{(p)} = \mathbf{R}_n \mathbf{U}_n^{(p)}$ and $\mathbf{F}_{n-1}^{(p)} = \mathbf{R}_{n-1} \mathbf{U}_{n-1}^{(p)}$. Although this equation is exact evaluation of small strain from deformation gradients, it is ill-advised numerically because it finds incremental strain by subtracting two non-incremental tensors (round-off error is likely). To eliminate this problem, we found a different decomposition to work better. The updated total deformation gradient is decomposed as

$$\mathbf{F}_n^{(p)} = d\mathbf{R} d\mathbf{U} \mathbf{R}_{n-1}^{(p)} \mathbf{U}_{n-1}^{(p)} = d\mathbf{R} \mathbf{R}_{n-1}^{(p)} (\mathbf{R}_{n-1}^{(p)})^T d\mathbf{U} \mathbf{R}_{n-1}^{(p)} \mathbf{U}_{n-1}^{(p)} \approx \mathbf{R}_n^{(p)} \mathbf{U}_n^{(p)} \quad (51)$$

where

$$\mathbf{R}_n^{(p)} \approx d\mathbf{R}\mathbf{R}_{n-1}^{(p)} \quad \text{and} \quad \mathbf{U}_n^{(p)} \approx \mathbf{R}_{n-1}^{(p)T} d\mathbf{U}\mathbf{R}_{n-1}^{(p)} \mathbf{U}_{n-1}^{(p)} \quad (52)$$

These results are not exact in large deformation theory, but both are exact in the limit of small strains. The stably evaluated small strain increment becomes

$$d\boldsymbol{\epsilon} = (\mathbf{R}_{n-1}^T d\mathbf{U}\mathbf{R}_{n-1} - \mathbf{I}) \mathbf{U}_{n-1}^{(p)} \quad (53)$$

which provides improved results for incremental strains. This incremental strain and the subsequent algorithm are hypoelastic implementations of small-strain elasticity. The tracking of deformation gradient and use of polar decomposition allows the analysis to track large rotations better than simpler hypoelastic methods. Rotations are important when the crack plane rotates in a dynamic analysis (although none of the above examples had significant rotation).

The next step depends on current state of the particle which will be “undamaged” (before initiation occurs), “damaged” (while damage is evolving), or “failed” (post failure state). For “undamaged” particles, the only tasks are:

1. Find trial stress update in the initial axes using $\boldsymbol{\sigma}^{(trial)} = \mathbf{R}_{n-1}^T \boldsymbol{\sigma}_{n-1}^{(p)} \mathbf{R}_{n-1} + \mathbf{C} d\boldsymbol{\epsilon}_0$. If failure criterion has not been reached, finish update by standard methods for a never-damaged material.
2. If the failure surface has been reached, mark the particle as “damaged,” calculate (and store) rotation matrix, $\mathbf{R}_c^{(p)}$, as rotation from crack axis system where crack normal is along the x axis, to initial axes, calculate (and store) V_p/A_c . Note that A_c is intersection between the particle and a plane through the particle center with the determined crack normal. The straight-forward geometric calculations need to support any 2D or 3D particle or element geometries that might be encountered. Proceed to update methods for a “damaged” particle.

For “damaged” and “failed” particles, rotate $d\boldsymbol{\epsilon}$ and previous particle stress to the crack axis system as $d\boldsymbol{\epsilon} = \mathbf{R}_c^{(p)T} d\boldsymbol{\epsilon} \mathbf{R}_c^{(p)}$ and $\boldsymbol{\sigma}^{(0)} = \mathbf{R}_{tot}^T \boldsymbol{\sigma}_{n-1}^{(p)} \mathbf{R}_{tot}$, where $\mathbf{R}_{tot} = \mathbf{R}_{n-1}^{(p)} \mathbf{R}_c^{(p)}$ and find $d\boldsymbol{\epsilon}_n$ using Eq. (9). For “damaged” particles, normal and shear updates are independent. For normal tractions, the tasks are:

1. Find a trial normal traction $T_n^{(trial)} = \sigma_{xx}^{(0)} + (1 - d_n) C_{11} d\boldsymbol{\epsilon}_n$.
2. If $T_n^{(trial)} \leq \sigma_n f_n(\delta_n)$, the update is elastic; δ_n and d_n are unchanged and cracking strain increments are $d\boldsymbol{\epsilon}_{c,xx} = \max(d_n d\boldsymbol{\epsilon}_n, -\boldsymbol{\epsilon}_{c,xx})$ (where $\max()$ is to handle crack contact and $\boldsymbol{\epsilon}_{c,xx}$ is current cracking strain rotated into the crack axis system).
3. If $T_n^{(trial)} > \sigma_n f_n(\delta_n)$, then damage is evolving. Divide the increment into elastic ($d\boldsymbol{\epsilon}_n^{(1)}$) and damage evolution ($d\boldsymbol{\epsilon}_n^{(2)}$) increments using

$$d\boldsymbol{\epsilon}_n^{(2)} = \frac{T_n^{(trial)} - \sigma_n f_n(\delta_n)}{(1 - d_n) C_{11}} \quad \text{and} \quad d\boldsymbol{\epsilon}_n^{(1)} = d\boldsymbol{\epsilon}_n - d\boldsymbol{\epsilon}_n^{(2)} \quad (54)$$

The cracking strain increment becomes $d\boldsymbol{\epsilon}_{c,xx} = d_n d\boldsymbol{\epsilon}_n^{(1)} + d\delta_n$, where $d\delta_n$ is numerical solution to $d\boldsymbol{\epsilon}_n^{(2)} = d\delta_n + \boldsymbol{\epsilon}_{n0}(f_n(\delta_n + d\delta_n) - f_n(\delta_n))$ from Eq. (19) (for linear softening, the exact solution is $d\delta_n = d\boldsymbol{\epsilon}_n / (1 + \boldsymbol{\epsilon}_{n0} f'_n(\delta_n))$). The increment in dissipated energy is found from Eq. (31).

Shear traction update for 2D damaged particles is analogous to normal traction (except no need to check for contact) and therefore not repeated here. In 3D, shear updates are coupled by a shear stress failure surface:

1. If $\tau_{xy}^{(0)} < 0$ or $\tau_{xz}^{(0)} < 0$, change their sign and sign of $d\gamma_{xy}^{(0)}$ or $d\gamma_{xz}^{(0)}$.
2. Find trial shear tractions $T_{ij}^{(trial)} = \tau_{ij}^{(0)} + (1 - d_{ij}) G d\gamma_{ij}$ (for $ij = xy$ and xz)
3. If new shear stresses are within elastic region of the failure surface; δ_{ij} and d_{ij} are unchanged and cracking strain increment is $d\boldsymbol{\epsilon}_{c,ij} = d_{ij} d\gamma_{ij}$.
4. If new shear stresses are outside the failure surface, divide the increment in to elastic ($d\gamma_{ij}^{(1)} = \phi d\gamma_{ij}$) and damage evolution ($d\gamma_{ij}^{(2)} = (1 - \phi) d\gamma_{ij}$) increments. Here ϕ is fraction of the update to reach the current failure surface. It can be found by solving a quadratic equation (but requires care to be numerically stable in all cases). After partitioning, replace $\tau_{ij}^{(0)}$ with stress on the failure surface ($\tau_{ij}^{(0)} + G(1 - d_{ij}) d\gamma_{ij}^{(1)}$) and proceed to one of three following cases:

- (a) If $d\gamma_{xy} > 0$ and $d\gamma_{xz} > 0$: Replace $d\gamma_{ij}$ with $d\gamma_{ij}^{(2)}$ and solve Eqs. (21) and (23). They can be solved stably in a few steps using Newton's method. The cracking strain increments are $d\gamma_{c,ij} = d_{ij}d\gamma_{ij}^{(1)} + d\delta_{ij}$.
- (b) If $d\gamma_{xy} > 0$ but $d\gamma_{xz} < 0$: Replace $d\gamma_{xy}$ with $d\gamma_{xy}^{(2)}$ and solve Eq. (25). It can be solved exactly for linear softening or by a few Newton's method steps for other laws. The cracking strain increments are $d\gamma_{c,xy} = d_{xy}d\gamma_{xy}^{(1)} + d\delta_{xy}$, $d\gamma_{c,xz} = d_{xz}d\gamma_{xz}$, and $d\delta_{xz} = 0$.
- (c) If $d\gamma_{xz} > 0$ but $d\gamma_{xy} < 0$: Same as previous case but interchange xy and xz shear components.

For all options, the increments in dissipated energies are found from shear versions of Eq. (31).

5. If signs were changed in step 1, change sign of $d\gamma_{c,ij}$.

Whenever damage evolves, Eq. (34) (or some other criterion) is used to determine if the particle has become a “failed” particle. For “failed” particles, cracking strain increments are $d\epsilon_{c,xx} = \max(d\epsilon_n, -\epsilon_{c,xx})$ (to handle crack contact), $d\gamma_{c,xy} = d\gamma_{xy}$, and $d\gamma_{c,xz} = d\gamma_{xz}$.

The above steps find cracking strain and crack traction updates in the crack axis system. The full update finishes with:

1. Updated global particle cracking strain using $\boldsymbol{\epsilon}_c^{(p,n)} = d\mathbf{R}\boldsymbol{\epsilon}_c^{(p,n-1)}d\mathbf{R}^T + \mathbf{R}_{tot}d\boldsymbol{\epsilon}_c\mathbf{R}_{tot}^T$.
2. Combine crack traction increments with increments for other three components of stress

$$d\sigma_{yy} = C_{11} \left(d\epsilon_{yy} + \frac{\nu}{1+\nu} (d\epsilon_{xx} - d\epsilon_{c,xx} + d\epsilon_{zz}) \right) \quad (55)$$

$$d\sigma_{zz} = C_{11} \left(d\epsilon_{zz} + \frac{\nu}{1+\nu} (d\epsilon_{xx} - d\epsilon_{c,xx} + d\epsilon_{yy}) \right) \quad (56)$$

and $d\tau_{yz} = Gd\gamma_{yz}$ and then update global stress using $\boldsymbol{\sigma}^{(p,n)} = d\mathbf{R}\boldsymbol{\sigma}^{(p,n-1)}d\mathbf{R}^T + \mathbf{R}_{tot}d\boldsymbol{\sigma}\mathbf{R}_{tot}^T$.

These final particle updates are rotating the previous particle state by the rotation increment of this step, $d\mathbf{R}$, and then adding incremental cracking strains and stress after rotating them from crack axis system to global coordinates.